Large-magnitude Miocene extension of the Eocene Caetano caldera, Shoshone and Toiyabe Ranges, Nevada

Joseph P. Colgan
David A. John
U.S. Geological Survey, Menlo Park, California 94025, USA

Christopher D. Henry
Nevada Bureau of Mines and Geology, Reno, Nevada 89557, USA

Robert J. Fleck
U.S. Geological Survey, Menlo Park, California 94025, USA

ABSTRACT

Because major mineral deposits in north-central Nevada predate significant Basin and Range extension, a detailed understanding of the timing and kinematics of extensional faulting is necessary to place these deposits in their original structural context. The complexity of pre-Cenozoic deformation in northern Nevada makes restoring Basin and Range faulting difficult without locating well-dated, regionally extensive Cenozoic units that can be used to restore slip along normal faults. The goal of this study is to reconstruct extensional faulting in the Shoshone and northern Toiyabe Ranges by using Cenozoic rocks in and around the Caetano caldera, which formed ca. 33.8 Ma during eruption of the Caetano Tuff. The caldera filled with more than 4 km of intracaldera tuff during initial caldera-forming eruptions, and additional sedimentary and volcanic rocks subsequently filled the topographic depression left by the caldera collapse. These rocks are conformable over the interval 34–25 Ma, consistent with little, if any, extension during that time. The 34–25 Ma rocks were later cut by a set of closely spaced (1–3 km) normal faults that accommodated significant extension and footwall rotations of 40°–50°. Restored structural cross sections indicate that the present ~42 km (east-west) width of the Caetano caldera has been extended 110%, resulting in 22 ± 3 km westward translation of the Fish Creek Mountains relative to the southern Cortez Range. Major normal faults mapped within the caldera continue south and north along strike into the surrounding Paleozoic basement rocks; therefore it is likely that parts of surrounding areas are also significantly extended. Miocene (16–12 Ma) sedimentary rocks in the hanging walls of major normal faults include both fluvial/lacustrine facies and coarser alluvial fan deposits. Where exposed, the bases of the Miocene sedimentary sections are in angular conformity with underlying ~40°E tilted 34–25 Ma volcanic and sedimentary rocks. The distribution, composition, and geometry of these deposits are best explained by accumulation in a set of half-graben basins that formed in response to slip on basin-bounding faults. Extension thus appears to have taken place in the middle Miocene, beginning at or shortly after 16 Ma, and was mostly completed by 10–12 Ma. Fault blocks and basins formed during middle Miocene extension are cut by younger, more widely spaced, high-angle normal faults that began forming more recently than 10–12 Ma. These faults outline the modern basins and ranges in the study area and some have remained active into the Holocene.

Keywords: Basin and Range Province, Miocene, extensional tectonics, calderas.

INTRODUCTION

Many of the major mineral deposits in north-central Nevada (including the world-class Carlin-type gold deposits) formed during the Eocene–early Oligocene (e.g., Hofstra et al., 1999; Ressel and Henry, 2006) and thus predate major extension in the northern Basin and Range, which took place primarily during the Miocene (e.g., Dickinson, 2006). Mineral deposits and potential mineralized host rocks have been variably disrupted by this faulting; therefore understanding Basin and Range deformation in this region is key for placing these deposits in their original structural context and for locating unexposed deposits beneath sedimentary or structural cover. In this paper we focus on Cenozoic deformation of the southern Shoshone–northern Toiyabe range area, site of the historic Cortez and Gold Acres deposits and the active (ca. 2007) Pipeline and Cortez Hills deposits.

Basin and Range deformation in this region is difficult to quantify, because exposed bedrock consists primarily of Paleozoic siliceous "western facies" rocks of the Roberts Mountains allochthon. These highly deformed, thrust-imbricated slices of argillite, quartzite, chert, and greenstone are the product of a complex history of Late Paleozoic contractional deformation overprinted by Cenozoic extension (e.g., Roberts et al., 1958; Gilluly and Gates, 1965). These rocks tend to be poorly exposed and offer few reliable stratigraphic markers that can be used to restore slip along normal faults. To understand Cenozoic extension, it is thus desirable to find well-dated, regionally extensive, pre-extensional Cenozoic rocks that can be matched across normal faults and used to restore extension of the underlying Paleozoic units.

The most extensive Cenozoic unit in the study area is the late Eocene Caetano Tuff (Gilluly and Masursky, 1965), exposed in the northern Toiyabe and southern Shoshone Ranges (Fig. 1). It was originally interpreted as filling the eastern part of an east-west–trending, ~90

jcolgan@usgs.gov

Geosphere; February 2008; v. 4; no. 1; p. 107–130; doi: 10.1130/GES00115.1; 11 figures; 4 tables; 1 plate.

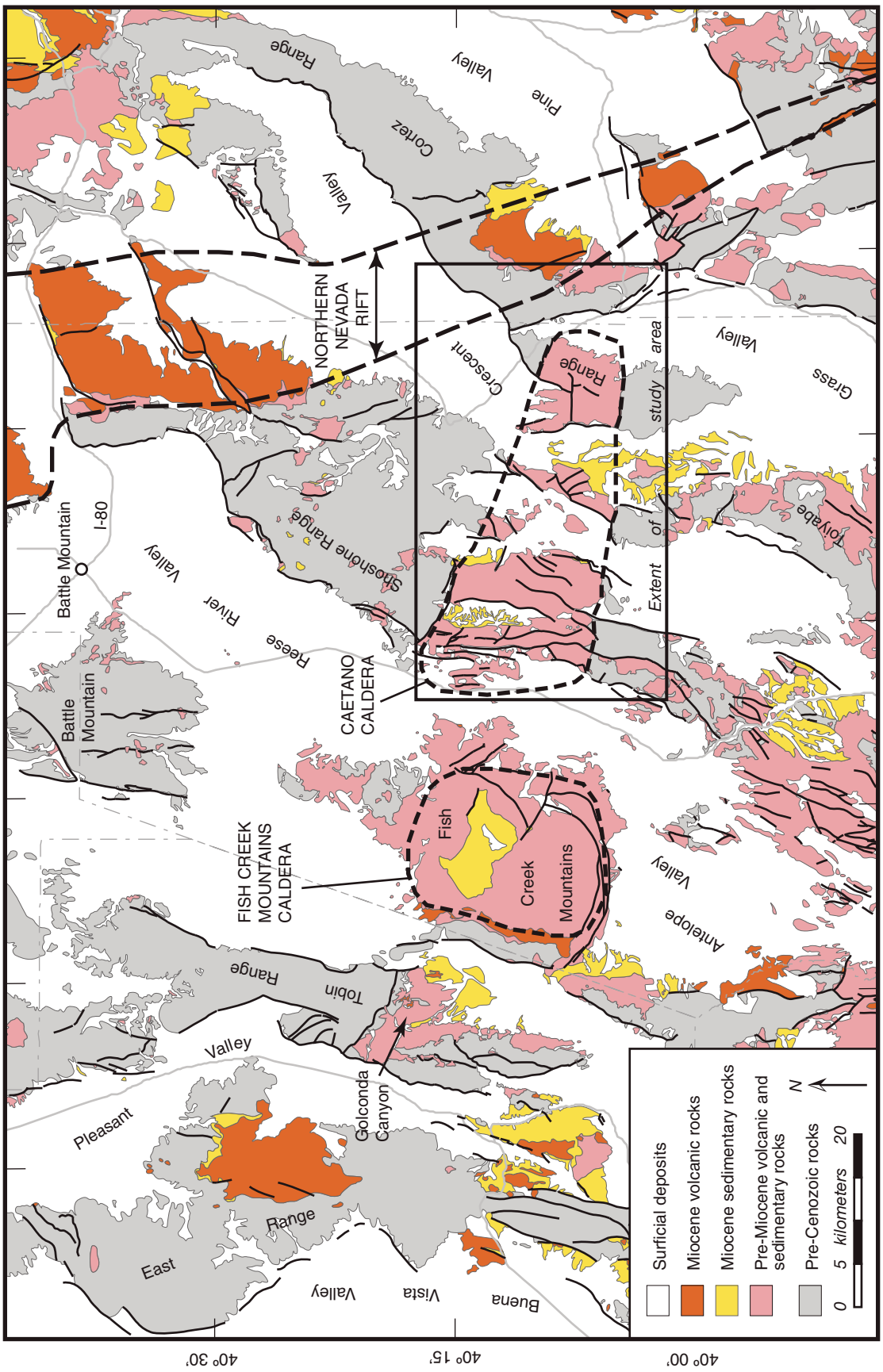

Figure 1. Geologic map of north-central Nevada, showing location of study area (Figs. 2, 9, and Plate 1) and other features discussed in the text. Geology simplified from Stewart and Carlson (1978).

× 20 km "volcano-tectonic trough" (Masursky, 1960; Burke and McKee, 1979). The western part of this "trough" has since been shown to consist of the structurally intact Fish Creek Mountains caldera (Fig. 1; McKee, 1970), dated to 24.72 ± 0.05 Ma (John et al., 2008). New geologic mapping, geochronology, and geochemical data indicate a similar caldera origin for the Caetano Tuff in the eastern part of the "trough," referred to hereafter as the Caetano caldera (this study; John et al., 2008). The present east-west elongation of the Caetano caldera (Figs. 1 and 2) is the result of east-west extension along north-striking normal faults, making the caldera an ideal strain marker for restoring later Cenozoic deformation.

John et al. (2008) present detailed field observations, geochemical data, and $^{40}Ar/^{39}Ar$ age data that establish an ~33.8 Ma age for the Caetano Tuff and demonstrate that it fills a structurally dismembered caldera (all $^{40}Ar/^{39}Ar$ dates in this paper are referenced to sanidine from the Fish Canyon Tuff with an assigned age of 28.02 Ma (Renne et al., 1998)). The purpose of this paper is to restore deformation of the caldera and thereby establish the timing and kinematics of Basin and Range extension in this region. We present a new geologic map and cross-sections (Plate 1) that document the magnitude and structural style of extension, together with new $^{40}Ar/^{39}Ar$ dates and tephra correlations from synextensional basins that establish the timing of faulting.

We conclude that the ca. 34 Ma Caetano caldera remained undeformed until the middle Miocene (ca. 16 Ma), at which point it was dismembered by large-magnitude, roughly east-west extension along north-striking normal faults that accommodated ~110% (~22 km) extension. Extension began ca. 16 Ma and took place in two main phases. We interpret 16–12 Ma sedimentary rocks to record large-magnitude middle Miocene extension and tilting of the Caetano caldera. Fault blocks and basins formed during middle Miocene extension were subsequently cut by a second generation of more widely spaced, high-angle normal faults that strike more northeast. The onset of younger faulting is not well established but is thought to be younger than ca. 10 Ma.

GEOLOGIC SETTING

In the following section, map units in parentheses refer to designations on the schematic stratigraphic column (Fig. 3), geologic map (Plate 1), and restored cross sections (Fig. 4). Geographic locations discussed in the text can be found in Figure 2 in addition to Plate 1. Plate 1 was compiled from new 1:24,000-scale geologic mapping of key localities (John et al., 2008), new 1:100,000-scale mapping of the caldera fill and Miocene sedimentary rocks (this study; John et al., 2008), and published geologic maps of the (mostly Paleozoic) rocks outside the caldera (sources listed in Plate 1).

Pre-Cenozoic Rocks

Exposed pre-Cenozoic basement in the southern Shoshone Range and northern Toiyabe Range (Fig. 2) consists primarily of lower Paleozoic (Upper Cambrian–Devonian) siliceous rocks of the Roberts Mountains allochthon (the upper plate), deposited in a deep ocean basin west of the North American continent and thrust eastward onto the continental shelf during the Late Devonian–Mississippian Antler orogeny (e.g., Roberts et al., 1958; Miller et al., 1992). These rocks have been divided into several formal and informal units by different authors; the most extensive of these include the Valmy Formation (argillite, quartzite, chert, greenstone; Roberts, 1951), Vinini Formation (argillite, quartzite, shale, chert; Merriam and Anderson, 1942), Slaven Chert, and Elder Sandstone (Gilluly and Gates, 1965). Within the upper plate, these units are repeated by numerous thrust faults and highly deformed at both outcrop and map scale (e.g., Gilluly and Gates, 1965). For the purpose of this study we consider these rocks to represent a single tectonic-stratigraphic package (Pzrm). In the northwestern part of the study area, we estimate that the upper plate was no more than ~2 km thick in the middle Miocene, although an unknown amount may have been removed by erosion before that time.

Underlying lower plate rocks (Pzlc) of the lower Paleozoic (Cambrian–Devonian) continental shelf (predominantly carbonate) are locally exposed in structural windows beneath the siliceous upper plate (Plate 1). In the southern Cortez Range, this sequence is at least 1.8 km thick with Cambrian rocks exposed at the base (Gilluly and Masursky, 1965). Lower plate carbonate rocks are an important host rock for the major gold deposits in the area, including the giant Pipeline deposit (2005 reserves ~11 Moz; past production ~9 Moz; Muntean, 2006). In the southern Cortez Range, the lower plate was exposed by mid-Tertiary erosion prior to extensional faulting (Gilluly and Masursky, 1965; John et al., 2008), but we argue here that some lower-plate windows may be exhumed in the footwalls of Miocene normal faults; this interpretation is discussed in a later section.

Upper Paleozoic rocks deposited unconformably on the Roberts Mountains allochthon following its emplacement—the Antler overlap assemblage—have been described by Moore et al. (2000) and Racheboeuf et al. (2004) in the southwestern part of the study area (Pzo). Equivalent units are exposed in the south-central Cortez Range (Fig. 1) to the northeast of the study area (Muffler, 1964). In the southwestern Shoshone Range, these rocks were overthrust in the Late Permian–Early Triassic by deep-water siliceous rocks of the Golconda allochthon (Pzg; Moore et al., 2005).

Cenozoic Rocks that Predate the Caetano Caldera

Few Cenozoic rocks in the study area are known to predate eruption of the Caetano Tuff and formation of the Caetano caldera. Sparse, undated andesitic lava flows are exposed on the caldera floor in the Toiyabe Range (Figs. 2 and 3; included in unit Tad; note that this unit also includes post-caldera lavas). Coarse clastic sediments containing abundant carbonate clasts derived from lower-plate rocks are exposed on the caldera floor near Wenban Spring (Fig. 2). These exposures may correlate with an extensive but poorly exposed >400-m-thick gravel deposit filling a paleovalley in the southern Cortez Range (Tog). To the north of our study area, local outcrops of outflow tuff previously mapped as Caetano Tuff (Stewart and McKee, 1977; Doebrich, 1995) are demonstrated by John et al. (2008) to be the tuff of Cove Mine, a similar but petrographically and geochemically distinct, slightly older (34.2 Ma) tuff that predates the Caetano caldera. Southwest of Wilson Pass in the Shoshone Range (Fig. 2), a small outcrop of the tuff of Cove Mine (Tcm) overlies a small outcrop of mafic lava (Tob). Both of these units are stratigraphically beneath the lower intracaldera cooling unit of the Caetano Tuff, and thus represent the floor of the caldera (discussed in detail by John et al., 2008).

Caetano Tuff and Related Units

Detailed petrographic data, geochemical analyses, and $^{40}Ar/^{39}Ar$ age data for the Caetano Tuff and related units are presented in a companion paper (John et al., 2008). Here we summarize aspects of these units relevant to our discussion of extensional faulting.

Intracaldera Tuff: Lower Unit

Most of the intracaldera Caetano Tuff is a single compound cooling unit as much as 3.4 km thick (Tcl), although the top and bottom of the caldera fill are never exposed in the same structural block. For the purpose of this study, we conservatively estimate that this unit is as thick as 3.6 km, although the maximum thickness may be slightly greater (John et al., 2008). The tuff

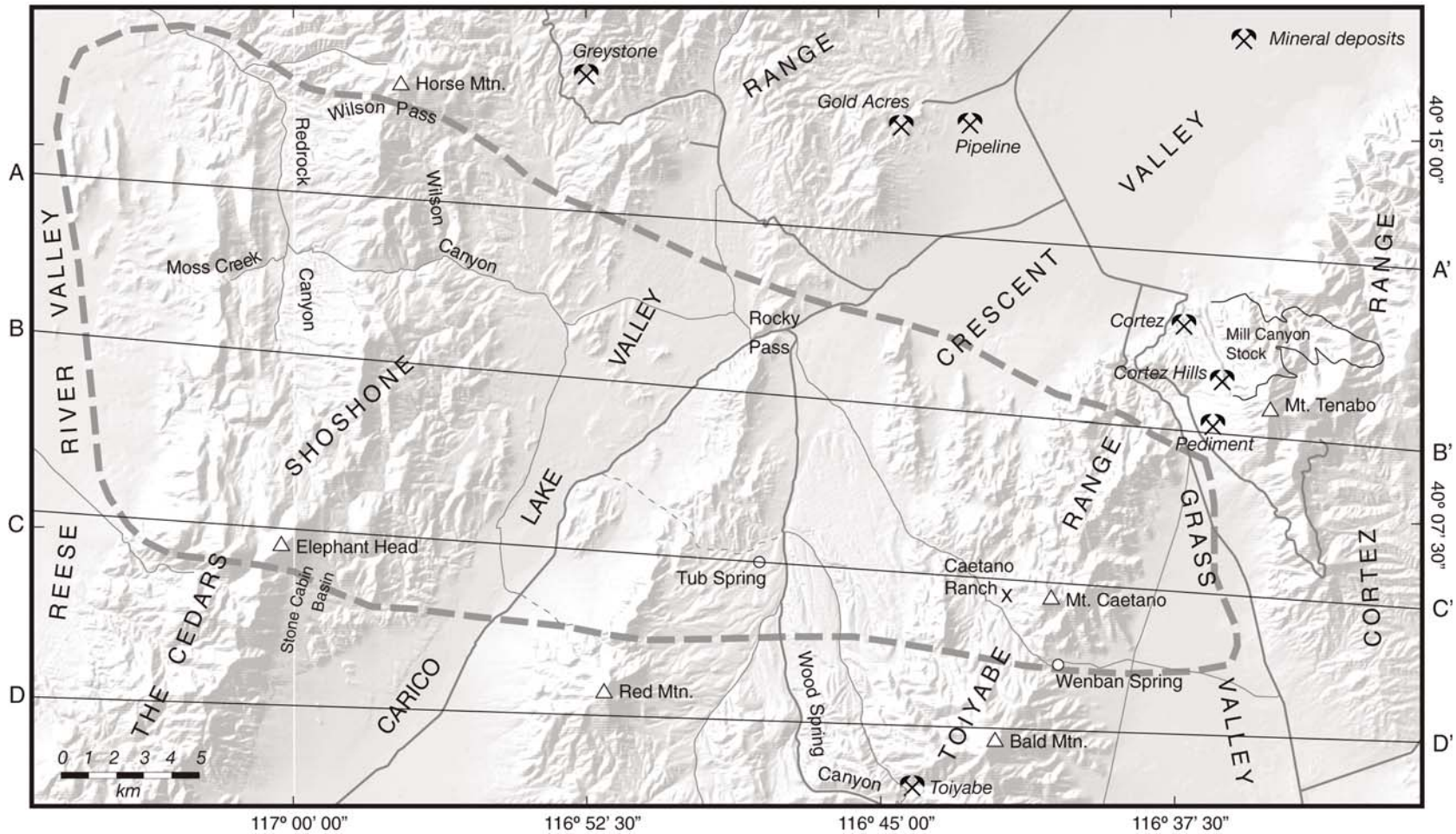

Figure 2. Shaded-relief map of study area (same extent as Fig. 9 and Plate 1), showing location of cross sections, geographic features, and mineral deposits discussed in the text. Dashed gray line is approximate extent of Caetano caldera. Gray lines are improved gravel (bold) and dirt roads (thin, solid and dashed). Base map same as Plate 1.

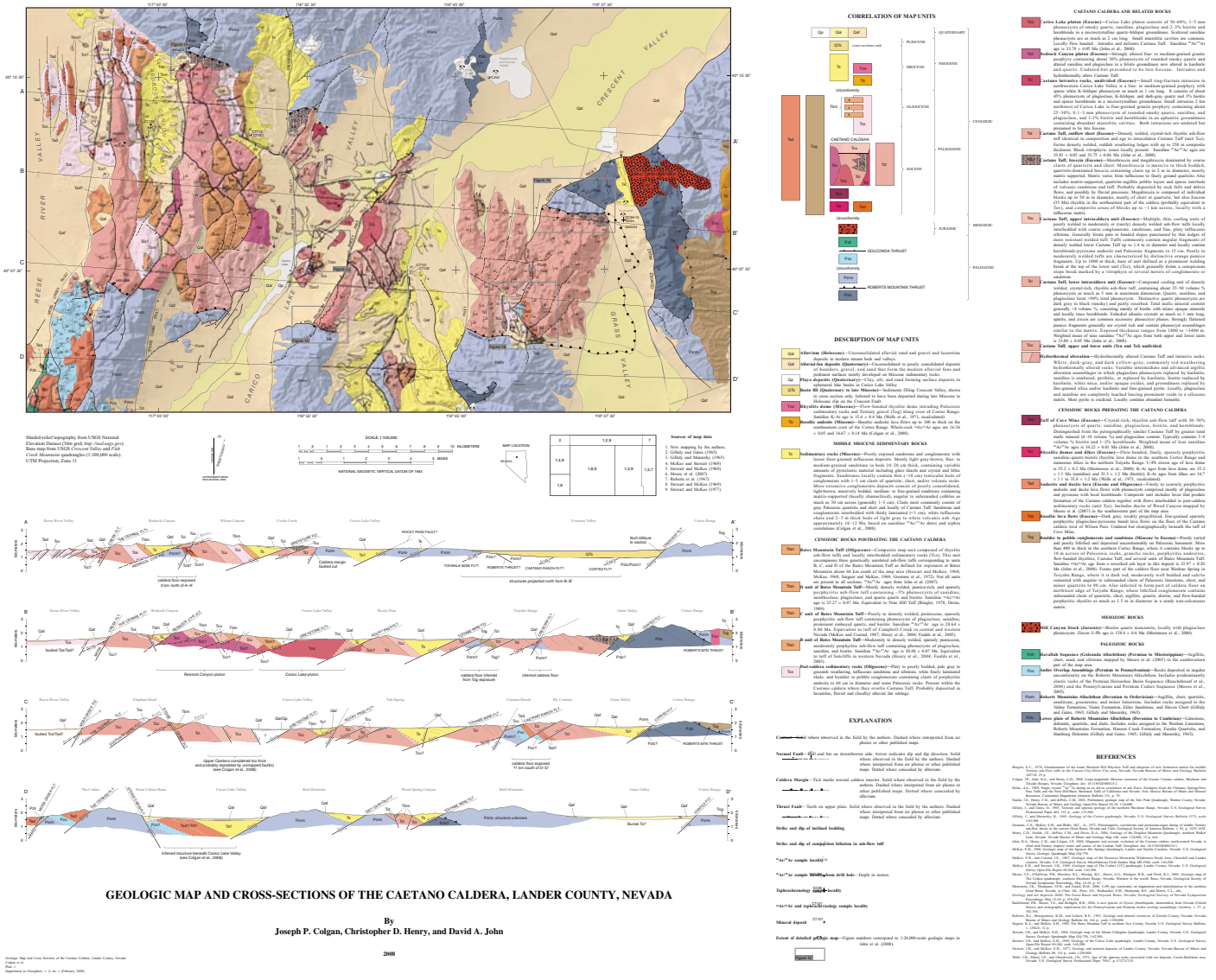

Plate 1. Colgan, J.P., Henry, C.D., and John, D.A., Geologic map and cross sections of the Caetano caldera, Lander County, Nevada, scale 1:100:000. If you are viewing the PDF of this paper or reading it offline, please visit http://dx.doi.org/10.1130/GES00115.S1 or the full-text article on www.gsajournals.org to access the full-size file of Plate 1.

in the eastern part of the caldera in the northern Toiyabe Range is relatively fresh, with vitrophyre locally preserved at the base. In contrast, the intracaldera tuff west of Carico Lake Valley (Fig. 2) is strongly hydrothermally altered; in some cases, it is difficult to tell if the rock was formerly extrusive or a shallow intrusion.

Intracaldera Tuff: Upper Unit

A distinct cooling break is present in the upper part of the intracaldera Caetano Tuff, most prominently exposed between Rocky Pass and Red Mountain in a series of small fault blocks west of Tub Spring (Fig. 2). Above this cooling break, the Caetano Tuff consists of as much as 1000 m of generally poorly exposed, poorly welded ash-flow tuff, locally interbedded with finely laminated tuffaceous siltstone and sandstone. Thin (5–10 m) ledges of densely welded tuff within this unit are geochemically and petrographically similar to the main intracaldera Caetano Tuff, and yield statistically indistinguishable $^{40}Ar/^{39}Ar$ ages (John et al., 2008). Where exposed, this sequence is a useful marker for restoring slip on normal faults, and we designate all caldera fill above the top of the lower cooling unit (Tcl) as a separate map unit (Tcu). Both the upper and lower units are hydrothermally altered in the western part of the caldera, and, where we have not mapped them in detail, they are shown as intracaldera tuff, undivided (Tcc).

Breccia

Large (>10 m) breccia blocks and crudely bedded sheets composed of crushed and broken Paleozoic quartzite and chert (locally with a tuffaceous matrix) are exposed along the margins of the caldera, consistent with catastrophic collapse during eruption of the Caetano Tuff. Breccia deposits large enough to be shown in Plate 1 are designated "Tcb,"

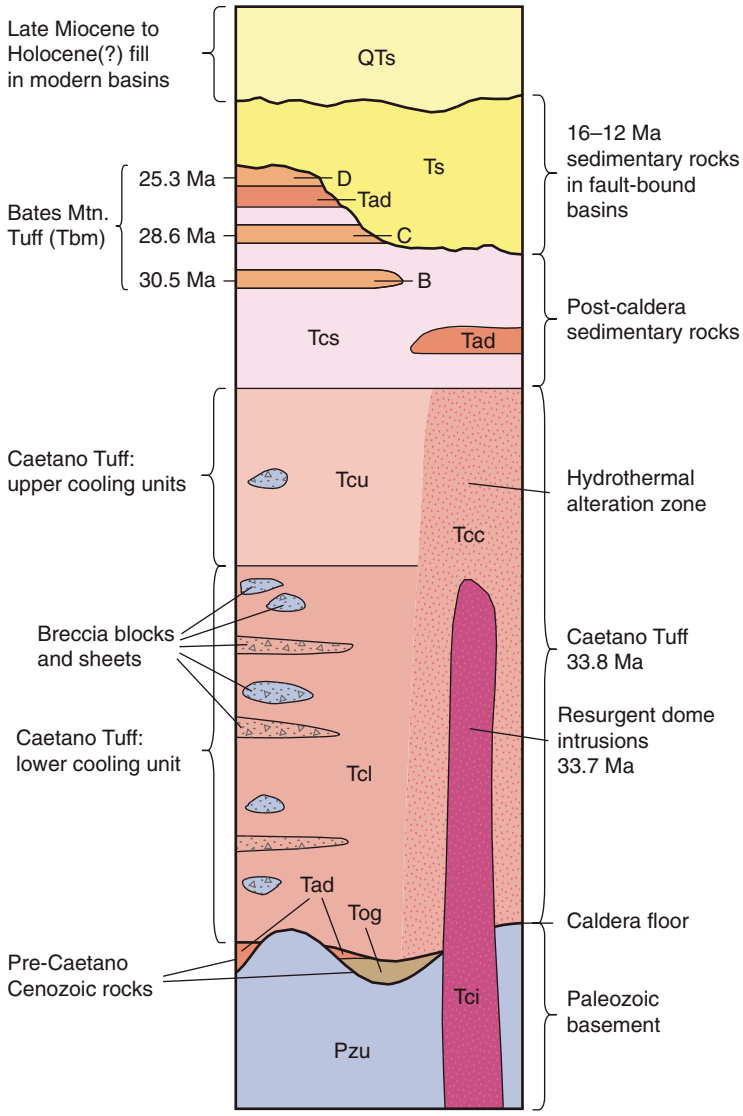

Figure 3. Schematic stratigraphic column for rocks in and around the Caetano caldera. Thickness of units not to scale. Unit colors and symbols same as Plate 1. Modified from John et al. (2008).

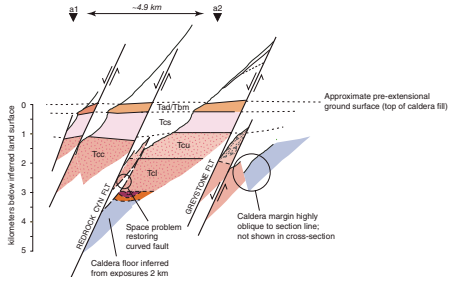

Figure 4. Restored cross sections A–A' (western part only), B–B', and C–C'. Sections reproduced directly from 1:100,000 scale geologic map (Plate 1). Lithologic units, colors, and symbols same as Plate 1 and Figure 3. FLT—fault; CYN—canyon. If you are viewing the PDF of this paper or reading it offline, please visit http://dx.doi.org/10.1130/GES00115.S2 or the full-text article on www.gsajournals.org to access the full-size file of Figure 4.

but they are locally present elsewhere along the caldera margins.

Intrusive Rocks

The central part of the caldera in Carico Lake Valley (Fig. 2) is underlain by the Carico Lake pluton, a poorly exposed granite porphyry (Tcic) that intrudes and deforms the surrounding intracaldera tuff. This granite is dated as 33.78 ± 0.05 Ma (^{40}Ar/^{39}Ar sanidine; John et al., 2008), and we interpret it to represent a resurgent intrusion derived from the same magma chamber that produced the Caetano Tuff. The Redrock Canyon pluton (Tcir) crops out sporadically across the western part of the caldera between Redrock Canyon and Carico Lake Valley (Fig. 2), where it intrudes the altered upper unit of the Caetano Tuff. This intrusion is strongly altered, and John et al. (2008) infer that it was the source of heat and/or hydrothermal fluids that altered the western part of the caldera.

Outflow Sheet

Outside the caldera, the Caetano Tuff is locally present within the study area as an outflow sheet generally deposited on pre-Cenozoic basement to the south and west of the caldera. The outflow sheet, shown as a separate unit (Tct) in Plate 1, is as much as 300 m thick where it fills paleotopography in Golconda Canyon in the Tobin Range (Fig. 1; Gonsior and Dilles, 2008; John et al., 2008).

Oligocene Rocks Overlying the Caetano Tuff

Within the caldera, the Caetano Tuff is locally overlain by 500–1000 m of tuffaceous sedimentary rocks (Tcs). These rocks are present only within the mapped outline of the caldera and are thickest along its edges (primarily the northwestern margin). We interpret these rocks to have been deposited in the topographic depression created by caldera collapse, in lacustrine and fluvial environments (John et al., 2008). The sedimentary rocks are overlain by, and interbedded with, the 25–30 Ma Bates Mountain Tuff (Tbm, described below), and are thus early Oligocene in age. They are shown separately from Tbm in Plate 1 where they are extensive enough to be mapped as a distinct unit.

The Bates Mountain Tuff as originally defined by Stewart and McKee (1968) actually consists of several genetically unrelated tuffs. In the study area, these tuffs include Bates Mountain B (30.48 ± 0.06 Ma), equivalent to the tuff of Sutcliffe in western Nevada (Henry et al., 2004; Faulds et al., 2003), Bates Mountain C (28.64 ± 0.07 Ma), equivalent to the tuff of Campbell Creek in central and western Nevada (Henry et al., 2004; Faulds et al., 2003; McKee and Conrad, 1987), and Bates Mountain D (25.27 ± 0.07 Ma), equivalent to the widespread Nine Hill Tuff (Bingler, 1978; Deino, 1989). Not all units are present at all localities, and the individual ash-flow sheets are interbedded with sedimentary rocks (Tcs). No angular discordance is evident within this

sequence of tuffs, or between them and the underlying sedimentary rocks and intracaldera Caetano Tuff. For the purpose of discussing subsequent deformation, it is convenient to refer to all rocks (including interbedded sedimentary rocks) between the stratigraphically lowest and highest Bates Mountain Tuff in a given section as a single unit, the 25–30 Ma Bates Mountain Tuff (Tbm). The composite sequence of Bates Mountain Tuff and interbedded sedimentary rocks may be as much as 300 m thick. Within the study area, the Bates Mountain Tuff is locally present outside the caldera, where it is deposited on outflow Caetano Tuff (Tct) or older lava flows (Tad).

In the western part of the study area, the Bates Mountain Tuff is interbedded with undated andestic and/or dacitic lava flows (Tad) mapped by Stewart and McKee (1977) and Moore et al. (2005). These flows are present both above and beneath the Bates Mountain Tuff, whereas similar lavas (the dacite of Wood Canyon) on the west side of the Cedars fault (Plate 1) are stratigraphically between the Bates Mountain Tuff and the Caetano Tuff (Moore et al., 2005).

Miocene Sedimentary Rocks

Miocene (16–12 Ma) sedimentary rocks locally overlie older volcanic rocks throughout the study area. These deposits (unit Ts, Plate 1) crop out between the larger fault blocks, and we interpret them to have been deposited in hanging-wall basins during fault slip. Because they bear directly on the timing of deformation, they are discussed in more detail in a later section.

STRUCTURAL RECONSTRUCTION

Well-developed compaction foliation in intracaldera tuff provides a good marker for postemplacement tilting of the Caetano caldera, but there are no widespread or laterally continuous marker horizons within the densely welded, locally strongly altered, intracaldera tuff. Our structural reconstruction (Fig. 4) is therefore based on matching recognizable units that overlie the thick intracaldera tuff, primarily the Bates Mountain Tuff (Tbm), post-caldera sediments (Tcs), and the distinctive upper cooling units within intracaldera tuff (Tcu). In most cases, major faults in the study area are covered by younger deposits or cut by younger faults, and we do not know their present dip; the net effect of this uncertainty on our reconstruction is discussed at the end of this section.

Where faults are exposed or where they can be measured directly from map traces, they now dip moderately to gently west (~25°–35°) and hanging-wall cutoffs suggest initial dips of ~62°–72°. In other cases we estimate the minimum (present day) fault dip by projecting the fault plane above the footwall topography and using the dip of footwall rocks to infer initial dip, suggesting initial dips >55°–65°. Available constraints on the dip of major faults in the study area are listed in Table 1, and where necessary, we infer initial dip (usually 65°) using these known faults as a guide (details are given where relevant in the following discussion). The cross sections are restored as a series of rigid fault blocks, ignoring internal deformation (folding and/or bending) and possible slip on unidentified small faults. Locally, this leads to space problems where footwall tilt changes from block to block (Fig. 4), which we assume is accommodated by internal deformation of the fault blocks and/or the faults curving in the subsurface. In cross section, these uncertainties are assumed to be small relative to the uncertainty in fault dip.

In the following section, we describe extension of the Caetano caldera by restoring cross sections A–A' (western part only), B–B', and C–C' (Fig. 2; Plate 1). Extension of the surrounding Paleozoic rocks (including section D–D') is discussed in a separate section. The following discussions are keyed to the geologic map (Plate 1) and restored cross sections (Fig. 4), which are necessary for following our descriptions in the text.

Extension of the Caetano Caldera (Sections A–A', B–B', C–C')

Restored Structure along Section A–A′

The western margin of the caldera is buried beneath Reese River Valley, and the westernmost units exposed along A–A' are post-caldera sedimentary rocks (Tcs) overlain by lava flows (Tad) and cut by many small-offset, west-dipping normal faults. These rocks are dropped down to the west along the west-dipping Moss Creek fault. To the east of the Moss Creek fault, a conformable, 40°–50°E dipping sequence of Caetano Tuff (Tcc) and post-caldera sedimentary (Tcs) and volcanic rocks (Tbm and Tad) is exposed on the west side of Redrock Canyon. The modern floor of Reese River Valley is ~400 m lower than Redrock Canyon above Moss Creek, and Miocene sedimentary rocks (Ts) in Redrock Canyon are being eroded by modern streams that drain through Moss Creek canyon into Reese River Valley. We therefore infer that the Moss Creek fault is a late Miocene or younger fault with at least 400 m vertical offset along A–A' and show it dipping 60°W (based on exposed fault surfaces at the mouth of Moss Creek; Fig. 5A) and cutting an older, more gently dipping fault that accommodated tilting of the caldera sequence exposed at Moss Creek. This older fault may be a northern extension of the Cedars fault system exposed to the south, and we estimate it to dip ~20°W, based on an assumed initial dip of 65° relative to a footwall tilt of ~45°E.

To the east of Redrock Canyon, a similar section of 40°–45°E dipping intracaldera tuff (Tcu), post-caldera sedimentary rocks (Tcs), Bates Mountain Tuff (Tbm), and Miocene sedimentary rocks (Ts) is exposed south of Wilson Pass. This sequence overlies a small exposure

TABLE 1. FAULT DIP DATA

Fault	Method	Fault dip (°W)	Footwall dip (°E)	Hanging-wall dip (°E)	Initial dip (°W)
Greystone fault 7 km north of A–A′ (Fig. 5B)	Outcrop	35	unknown	unknown	unknown
Greystone fault along A–A′	Minimum dip	≥12	60 (?)	not exposed	≥72(?)
Unnamed fault along B–B′, just east of Redrock Canyon fault	3-point	18	33	45	63
Unnamed fault (Fig. 6B) along C–C′, east of Stone Cabin fault	Outcrop	27	50	30	57
Rocky Pass fault along B–B′	Minimum dip	≥25	40	not exposed	≥65
Caetano Ranch fault 2 km north of C–C′	Minimum dip	≥15	35	45	≥60
Caetano Ranch fault 400 m south of C–C′	Minimum dip	≥18	45	45	≥63
Toiyabe Mine fault 2 km south of C–C′	Minimum dip	≥15	45–50	not exposed	≥60–65
Cedars fault 1 km north of D–D′	3-point	35	23	38	72
Cedars fault along D–D′	Outcrop	40	unknown	15	≥55

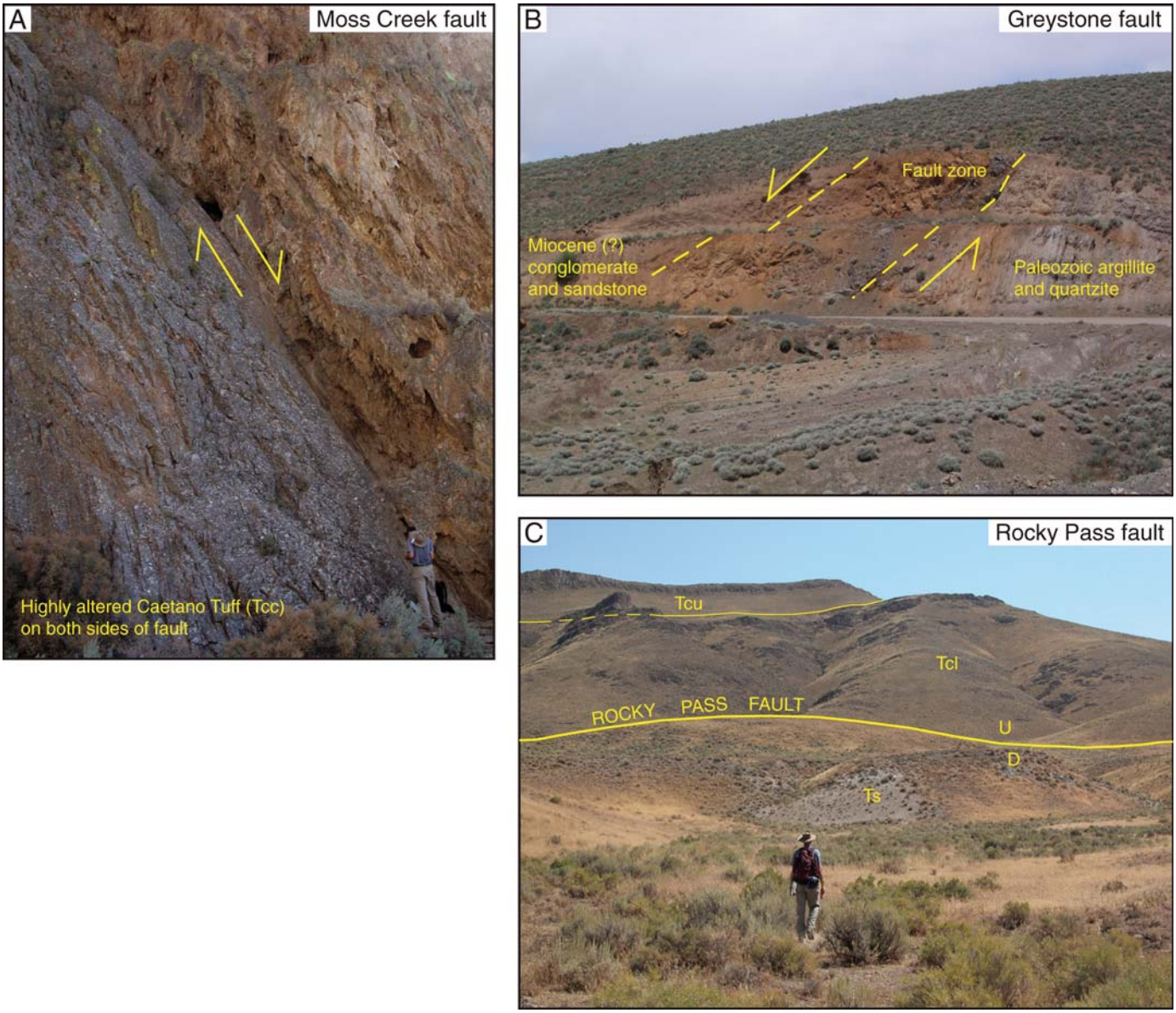

Figure 5. (A) View south of high-angle west-dipping normal fault at the mouth of Moss Creek Canyon. (B) View north of west-dipping Greystone fault in roadcut (~10 m high) 2 km north of Greystone Mine. (C) View east of west-dipping Rocky Pass fault, 2 km south of Rocky Pass. Ridge is 325 m above valley floor.

of the caldera floor (John et al., 2008) and is faulted against Miocene sedimentary rocks (Ts) in Redrock Canyon along the west-dipping Redrock Canyon fault. A second fault east of the Redrock Canyon fault forms a prominent topographic step but does not repeat the tuff of Cove Mine and probably has no more than a few hundred meters of slip. We therefore interpret this second fault as a younger, more steeply dipping (inferred 60°) fault. It cuts the older Redrock Canyon fault, which is inferred to dip ~20° based on an assumed initial dip of 65° and the ~45° tilt of its hanging wall and footwall blocks. After restoring ~100 m of slip on the unnamed small fault, ~6 km of slip on the Redrock Canyon fault is required to match the Bates Mountain Tuff on either side of Redrock Canyon.

Intracaldera tuff (Tcc and/or Tcu) and breccia (Tcb) are exposed east of Cooks Creek in the footwall of the Greystone fault, which is exposed ~7 km north of A–A' in several roadcuts along the haul road to the Greystone Mine. There, it dips ~35°W and places (Miocene?) alluvial fan deposits against brecciated Paleozoic chert and quartzite (Fig. 5B). Along Redrock Canyon, we assume a more gentle ~20° dip for the Greystone fault based on 70°–40° dipping Caetano Tuff and breccia sheets exposed south of the line of section. The extensive breccia deposit along the caldera margin here appears to be interbedded with the upper cooling units of the Caetano Tuff (Tcu), so we restore this block to just below the inferred base of the post-caldera rocks (Tcs and Tbm) to the west, requiring ~5 km of slip on the Greystone fault. The caldera margin is nearly parallel to line A–A' at this point and we do not attempt to accurately portray it on the cross section.

The footwall of the Greystone fault is covered by alluvium at the north end of Carico Lake Valley, and no known Cenozoic rocks are exposed farther east along A–A'. Undated, poorly exposed gravel deposits north of Rocky Pass may be Miocene sedimentary rocks (Ts?) in the hanging wall of the Rocky Pass fault system, although it is unclear where this fault (or faults) extends north into Paleozoic rocks. Approximately 3 km south of line A–A', 37°–43°E dipping Caetano Tuff (Tcl) crops out along the north wall of the caldera, suggesting that west-dipping faults continue at least several kilometers north in the Paleozoic rocks. Paleozoic rocks in this area are complexly faulted (Gilluly and Gates, 1965), and it is extremely difficult to tell whether faults have thrust or normal displacement, let alone their age. The eastern ~19 km of line A–A' is buried beneath late Miocene(?) to Holocene basin fill in Crescent Valley. On line A–A', we show the approximate position of faults exposed along line B–B' 4–5 km to the south, as they would project if they continued north beneath Crescent Valley.

Restoring the Caetano caldera over the western part of section A–A', between the surface trace of the Moss Creek fault (a1) and the surface trace of Greystone fault (a2), yields ~5.6 km of extension (10.5–4.9 km) or ~115% strain. Given the lack of Cenozoic marker units northeast of the caldera and the extent of young cover in Crescent Valley, it is impossible to restore the eastern ~30 km of the section.

Restored Structure along Section B–B'

West of the Moss Creek fault, line B–B' is covered by alluvium in Reese River Valley, although it is inferred at depth to consist of faulted post-caldera sedimentary rocks (Tcs) and lava flows (Tad) by analogy to line A–A'. The Moss Creek fault is assumed to dip ~60ºW and cut an older fault that dips ~25°W (assumed initial dip of 65°), with ~40°E dipping intracaldera Caetano Tuff, post-caldera sedimentary rocks (Tcs), and Bates Mountain Tuff (Tbm) in its footwall. This older fault may be the northern extension of the Cedars fault or fault system, and the footwall is locally complicated along B–B' by a minor down-to-the east fault that dies out to the north.

To the east of Redrock Canyon, line B–B' crosses the Redrock Canyon fault and two other west-dipping faults that drop 40°–45°E dipping sedimentary rocks (Tcs) and Bates Mountain Tuff down against highly altered intracaldera tuff (Tcc) and the Redrock Canyon pluton (Tcir). Redrock Canyon is bound on the east side by the Redrock Canyon fault, which places Miocene sedimentary rocks against the Redrock Canyon pluton. We assume a 35°W dip for the Redrock Canyon fault along B–B', somewhat less than along A–A', consistent with less steeply dipping Bates Mountain Tuff in its hanging wall. Approximately 2.5 km of slip on the Redrock Canyon fault, together with 2.5 km combined slip on the two gently west dipping faults to the east is required to restore the Bates Mountain Tuff (Tbm) on either side of Redrock Canyon. This system of west-dipping faults is cut at a high angle by two northeast-striking, down-to-the southeast faults that form prominent lineaments on aerial photographs but appear to have only a few hundred meters of offset at most.

Within Carico Lake Valley, line B–B' crosses alluvial cover and the Carico Lake pluton (Tci), interpreted as a resurgent intrusion within the Caetano caldera (John et al., 2008). In the low hills between lines B–B' and C–C', 35°E dipping Bates Mountain Tuff is exposed just south of the intrusion, requiring a west-dipping fault to bring it up relative to east-dipping exposures of Bates Mountain Tuff and sedimentary rocks (Tcs) to the west. We infer this fault to be a southern extension of the Greystone fault system extending south down Carico Lake Valley. Along B–B', this fault drops Caetano Tuff and overlying rocks down against the pluton, although it is unclear how far west the pluton extends in the subsurface. The east side of Carico Lake Valley is bound by the west-dipping Rocky Pass fault, which places 24°E dipping Miocene sedimentary rocks (Ts) against 40°–45°E dipping intracaldera Caetano Tuff (Tcl and Tcu) exposed along the steep ridge south of Rocky Pass (Fig. 5C). The Rocky Pass fault is not exposed, but is inferred to dip ~25°W, based on an assumed initial dip of 65° and a footwall tilt of 40° (Table 1). The exposed top of the upper Caetano Tuff (Tcu) in the footwall of the Rocky Pass fault is assumed to restore to a preextensional stratigraphic position just beneath the Bates Mountain Tuff. Approximately 8.5–9.0 km of total slip along the Rocky Pass fault and inferred Greystone fault is therefore required to restore the upper Caetano Tuff (Tcu) beneath the Bates Mountain Tuff (Tbm) in the southern Shoshone Range. To the east of Rocky Pass, the Caetano Tuff is assumed to be overlain by Miocene sedimentary rocks (Ts), which dip 10°–20°E where exposed along strike to the south.

The northern Toiyabe Range is bound to the west by the west-dipping Toiyabe Mine fault. The present dip of this fault is unknown, but we estimate ~20°–25°, assuming an initial dip of 65°–70° and a footwall tilt of 45°E, based on measured dips in the upper Caetano Tuff (Tcu) and overlying sedimentary rocks (Tcs) exposed 6 km to the south near Caetano Ranch. The footwall of the Toiyabe Mine fault along line B–B' consists almost entirely of densely welded intracaldera tuff (Tcl), which is cut by several small-offset, west-dipping faults assumed to have a geometry similar to that of the Toiyabe Mine fault. John et al. (2008) interpret a small exposure of conglomerate just east of the Toiyabe Mine fault to predate the Caetano Tuff, correlative with conglomerate (Tog) exposed on the floor of the caldera east of Caetano Ranch (2 km south of C–C'). The exposure of caldera floor portrayed in B–B' is based on this interpretation, assuming the conglomerate is no more than 400 m thick. Assuming that the lower Caetano Tuff is ~3.6 km thick (consistent with its >3.4 km thickness in the footwall of the Caetano Ranch fault just to the east), ~7–8 km of combined slip on the Toiyabe Mine fault and the next west-dipping fault to the east is required to exhume the caldera floor. We assume very little slip on the other two west-dipping faults, consistent with no additional exposures of the caldera floor to the east. Interpretation of the gravel deposit (Tog) as caldera floor affects the stratigraphic position of the restored footwall of the Toiyabe Mine fault (and thus the total slip on each fault), but has very little effect on the amount of extension.

The easternmost block in the northern Toiyabe Range is bound along B–B' by the southernmost trace of the Crescent fault, a young (late Miocene(?) to Holocene) high-angle fault that cuts the older, more gently dipping Caetano Ranch fault. We infer an initial dip of 65°W for the Caetano Ranch fault, which currently dips >15°–18° (Table 1). The amount of slip on the Crescent fault is not known, but is inferred to be small because it dies out 2–3 km to the south; we show ~500 m of slip in the cross section. South of B–B', the Caetano Tuff is unbroken by major faults and dips 35°–45°E. This is the greatest exposed thickness of the lower Caetano Tuff (~3.4 km), and we assume it to be close to the maximum thickness (inferred 3.6 km; John et al., 2008), although additional fill may be concealed upsection beneath northern Grass Valley. After restoring the Crescent fault, ~2 km of slip on the Caetano Ranch fault is required to restore this thick section of intracaldera tuff with similar exposures to the west, although this is dependent upon the caldera floor being exposed in the footwall of the Toiyabe Mine fault. The eastern margin of the caldera is shown in Plate 1 as the subsurface extent of the Caetano Tuff defined by Barrick Gold Corporation from geophysical and drill-hole data (K. Hart, 2006, written commun.).

The breccia deposit (Tcb) along the caldera margin in B–B' was mapped by Gilluly and Masursky (1965) as in-place Paleozoic rocks, but John et al. (2008) interpret it as megabreccia blocks of Paleozoic rocks within the caldera, on the basis of field relationships and drilling

data (R. Leonardson, 2007, oral commun.). Northern Grass Valley is bound to the east by the west-dipping Cortez fault, which drops Miocene conglomerate and sandstone down against lower-plate Paleozoic rocks intruded by the 158 Ma Mill Canyon Stock (Gilluly and Masursky, 1965). We estimate ~4 km of slip on the Cortez fault. Both the Cortez fault and Miocene sedimentary rocks in its footwall are cut by the younger Crescent fault, which strikes nearly east-west and dips 60°N where it truncates the northern end of Grass Valley at the Cortez Mine (Fig. 6A). The Cortez Range footwall block is structurally intact and tilted gently east-southeast. Miocene (16.7–16.4 Ma; Table A1) basalt flows on the crest of the range dip <10°SE, and lower-plate carbonate rocks adjacent to the Cortez fault dip as much as ~30°E (Gilluly and Masursky, 1965). We interpret the Cortez fault as the breakaway fault for the system of west-dipping faults that extended the Caetano caldera, with footwall tilt within the Cortez Range increasing toward the Cortez fault, possibly due to flexural uplift and bending of the Cortez Range footwall block during fault slip.

Restoration of section B–B', between the surface trace of the Moss Creek fault (b1) and the surface trace of the Cortez fault (b2), yields 20.0 km of extension (38.2–18.2 km), or ~112% strain.

Restored Structure along Section C–C'

The western end of line C–C' is covered by Reese River Valley and is close to the southern caldera margin, which parallels the section line. The west side of the Shoshone Range forms a steep front that rises 800 m above Reese River Valley, suggesting a somewhat greater amount of slip on the Moss Creek fault (we estimate ~1 km) than to the north (see B–B'). East of the Moss Creek fault, the Caetano Tuff dips 30°–40°E and

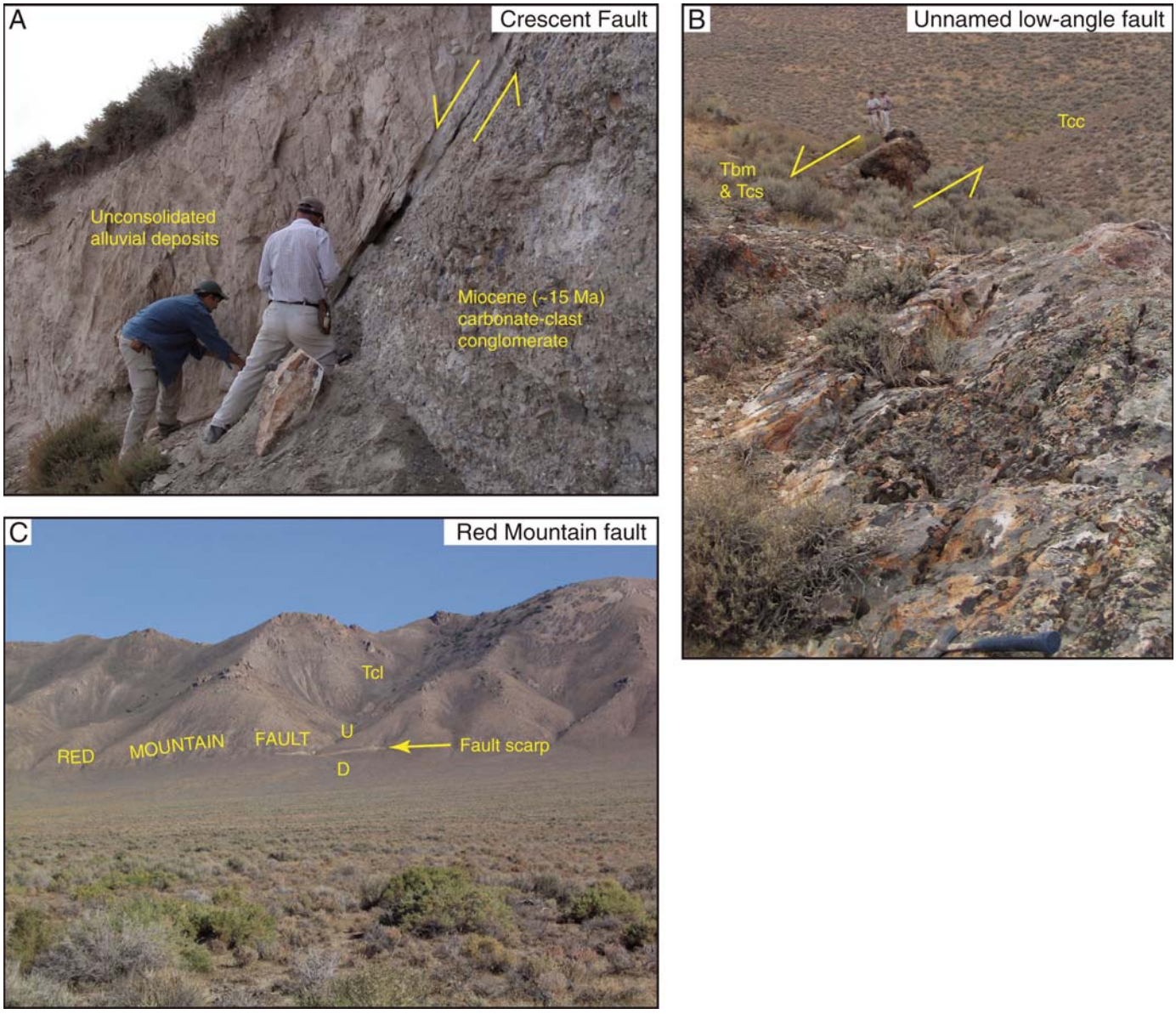

Figure 6. (A) View east of north-dipping Crescent fault at the Cortez Mine. (B) View north of west-dipping fault north of Stone Cabin Basin. (C) View east of Red Mountain fault on east side of Carico Lake Valley; note prominent fault scarp. Ridge along skyline is 300 m above valley floor. U—upthrown; D—downthrown.

is cut by two prominent north-striking faults. The Cedars fault dips 35°W as it cuts down the range front north of the section line. Along C–C' it is entirely within altered intracaldera tuff (Tcc), although subcrop of what may be post-caldera sedimentary rocks (Tcs) in the hanging wall suggests that it drops down the upper part of the caldera fill. To the east, the west-dipping Elephant Head fault drops Bates Mountain Tuff and post-caldera sedimentary rocks (Tcs) down against altered intracaldera tuff. The dip of this fault is not known, but we assume it to be similar to the Cedars fault (35°W; Table 1).

The east side of Elephant Head is bound by the down-to-the east Stone Cabin fault, which forms the west side of Carico Lake Valley to the south. Slip on this fault is inferred to increase from north to south with increasing topographic relief; at the latitude of C–C' we assume ~500 m of slip on this fault. To the east of the Stone Cabin fault, 30º–35ºE dipping Bates Mountain Tuff is faulted against Caetano Tuff along a 26°W dipping fault exposed in a small drainage (Fig. 6B). This is one of the few outcrop exposures of the gently west dipping faults that dismember the Caetano caldera. Intracaldera tuff (Tcl and Tcu) and breccia in the footwall of this fault dip ~50ºE. The fault must be cut to the west by the Stone Cabin fault, but the upthrown trace (dashed on the cross section) has not been identified or is not currently exposed (and is not shown on the map). To the east, the upper Caetano Tuff is cut by a high-angle, down-to-the east fault that places Bates Mountain Tuff against Caetano Tuff ~2 km north of line C–C'. The restored thickness of the upper Caetano Tuff between the Stone Cabin fault and Carico Lake Valley is >2 km (Fig. 4). Rather than being twice as thick here as its documented 500–1000 m thickness elsewhere, we think it more likely that the upper Caetano Tuff here is repeated by an unmapped down-to-the west fault. The west side of Carico Lake Valley is marked by young fault scarps that offset alluvial fans (Qaf) by several meters, and we show small offset of the fan deposits on the cross section.

Caetano Tuff and overlying rocks are exposed in a low hill just north of line C–C' in Carico Lake Valley. The Caetano Tuff here is strongly altered, brecciated, and displays an anomalous east-west strike and steep (70°–90°) dips, which we attribute to deformation during intrusion of the Carico Lake pluton (John et al., 2008). Deformed intracaldera tuff is overlain by Bates Mountain Tuff and post-caldera sedimentary rocks (Tcs) that dip ~30°E, requiring that they be bound by a west-dipping fault to bring them up relative to exposures of the same units to the west, although the exact location and geometry of this fault are concealed by alluvium. We infer a southern extension of the Greystone fault system dipping ~30°W. Approximately 5–6 km of total slip is required on the inferred Greystone fault and the exposed fault east of the Stone Cabin fault (shown in Fig. 6B) to restore the Bates Mountain Tuff in Carico Lake Valley with the outcrops just east of the Stone Cabin fault.

North of Red Mountain, the east side of Carico Lake Valley is bound by the Red Mountain fault, with a prominent scarp suggestive of recent (Holocene?) slip (Fig. 6C). The north-striking Red Mountain fault makes an ~90° bend to strike east-west at the latitude of the caldera margin, and we infer that it reactivated an ~2-km-long section of the original caldera-bounding fault. The Red Mountain fault cuts an older, ~40ºW dipping fault that is exposed for 3–4 km along the range front north of Red Mountain. This fault is entirely within altered intracaldera Caetano Tuff dipping 40°–45°E, so we infer the presence of an additional fault necessary to bring the Bates Mountain Tuff in Carico Lake Valley down relative to Red Mountain; this fault is shown on C–C' as a 25°W dipping extension of the Rocky Pass fault. Above the lower Caetano Tuff, the upper unit (Tcu) dips 40°–45°E, and, after restoring 200–300 m of slip on the Red Mountain fault, these exposures are restored by ~2.6 km of slip along the Rocky Pass fault to a position just beneath the Bates Mountain Tuff to the west. Between Carico Lake Valley and Tub Spring, the upper unit (Tcu) is repeated by several small west-dipping faults; ~1.5–2 km total slip is required on this set of faults to restore the upper cooling units with exposures to the west. To the east and southeast, these fault blocks are overlain by Miocene sedimentary rocks (Ts) that dip 10º–20ºE.

The Toiyabe Range along section C–C' is bound by the Toiyabe Mine fault, which (as along B–B') is inferred to dip ~20°W beneath Miocene sedimentary rocks, based on 40°–60° dips in Caetano Tuff and in post-caldera sedimentary rocks in its footwall and an assumed 65° initial dip. The footwall of the Toiyabe Mine fault exposes ~1.4 km of intracaldera Caetano Tuff overlain by 100–200 m of post-caldera sedimentary rocks (Tcs); the sedimentary rocks may continue upsection beneath the large area of alluvium north of the caldera margin. Approximately 5–6 km of slip is required on the Toiyabe Mine fault to restore these exposures adjacent to the upper cooling unit west of Tub Spring, although the displacement could be partitioned onto additional faults buried beneath Miocene sedimentary rocks (or that cut the sediments but are not exposed).

The northern Toiyabe Range is split by the north-striking Caetano Ranch fault, which is cut along line D–D' by a northwest-striking, down-to-the southwest fault with <500 m of offset. The Caetano Ranch fault drops upper Caetano Tuff down against Paleozoic rocks overlain by ~200 m of Tertiary andesite lava flows. This is the only significant exposure of the caldera floor in the study area, and is discussed in more detail by John et al. (2008). To the east of the Caetano Ranch fault, another west-dipping fault offsets the caldera floor 400–500 m; the subsurface geometry of this fault is projected onto section C–C' from ~2 km to the south. The footwall of this fault exposes ~2 km of intracaldera tuff, although a greater thickness is likely present beneath Grass Valley (as shown in the cross section). The location of the eastern caldera margin beneath Grass Valley is shown as determined by Barrick Gold Corporation from potential field and drill-hole data (K. Hart, 2006, written commun.). A minimum of ~3.5 km of slip is required on the Caetano Ranch fault, but this would make the main intracaldera cooling unit only 2.4 km thick. If instead the main cooling unit is assumed to be ~3.6 km thick, comparable to the incomplete 3.4 km section exposed along strike to the north, then ~5 km of slip is required.

The footwall of the Cortez fault along our section C–C' was originally mapped by Gilluly and Masursky (1965) as an upright fold in the Roberts Mountains thrust, with upper-plate units exposed along the range front in the western limb. We reinterpret these exposures of upper-plate rocks as being displaced down by ~2 km of slip on a west-dipping normal fault that intersects line D–D' obliquely and displays an apparent shallow dip in cross section. We estimate a combined 3.5–4 km of slip on this fault and the Cortez fault.

Restoration of section C–C', between the surface trace of the Moss Creek fault (c1) and the surface trace of the Cortez fault (c2), yields 21.7 km of extension (40.9–19.2), or ~113% strain.

Structural Reconstruction: Summary

The primary source of uncertainty in drawing and restoring the cross sections arises from the need to make assumptions about the dip of many of the major normal faults. To translate this uncertainty in fault geometry into uncertainty in the magnitude of extension, we consider that extension of the caldera occurred along a set of parallel, rotating, domino-style normal faults, which is a good approximation of the mapped geology. The magnitude of strain then depends on the present tilt of the fault blocks (α) and the initial fault dip (θ) by the following relationship (modified from Thompson, 1960):

$$Strain(\%) = \left(\frac{\sin(\theta)}{\sin(\theta-\alpha)} - 1\right) * 100 \quad (1)$$

Figure 7 is a plot of all compaction foliation and bedding attitudes from pre–25 Ma Cenozoic rocks within the Caetano caldera measured during this study; they strike roughly north (N11°E) and dip ~30°–50°E. These measurements are not evenly distributed across the study area and thus may be a better indication of the range of possible dips rather than the average, but for the sake of this exercise we estimate 40° of block rotation across the caldera (the average of all measurements). Figure 8 then shows the effect of assumed initial fault dip on the restored width of the (now) 42-km-wide caldera. Based on the data in Table 1, we assume that most major faults in the study area had initial dips of 60°–70°, yielding an original caldera width of 17–23 km, corresponding to 90%–150% strain (technically, equation 1 yields an original width of 19.6 +2.7/–3.0 km). Available constraints on the dip of major normal faults (Table 1) appear to rule out initial fault dips <~60°, but dips >70° are permitted for some of the unknown faults, which would lead to somewhat less total strain.

Based on restored cross sections B–B' and C–C' (~110% strain for assumed initial fault dips of 65°; Fig. 4), and the above analysis (±3 km extension for initial fault dips of 60°–70°), we conclude that the present 42 km east-west dimension of the Caetano caldera has undergone roughly 110% strain, representing 22 ± 3 km westward translation of the Fish Creek Mountains relative to the Cortez Range (Fig. 1). The preextensional Caetano caldera was thus roughly equant, ~10–17 km north-south by 20 km east-west, with the east side (10 km north-south) apparently narrower than the west (17 km north-south). Extension was taken up on a set of initially high angle, closely spaced (1–3 km), west-dipping normal faults that underwent 35°–50° of block rotation. The consistent north-strike (N11ºE) of tilted units in the footwall blocks of these faults (Fig. 7) is consistent with major extension oriented approximately east-west or slightly northwest. These earlier faults are cut, commonly at oblique angles, by a second set of more widely spaced, high-angle faults that locally have significant vertical offset but do not appear to have accommodated much horizontal extension. In restoring the cross sections, we assume negligable tilting associated with slip on this younger set of faults. The largest of them, the Crescent fault (Plate 1), has ~6° of footwall tilt despite 2–3 km of vertical offset (Muffler, 1964; Gilluly and Masursky, 1965). Therefore, we believe this is a reasonable assumption for the much smaller high-angle faults on our cross sections. The major faults appear to cut the caldera margin and continue north and south into the surrounding Paleozoic rocks, and we discuss the probability of extension outside the caldera in a later section.

MIOCENE SEDIMENTARY BASINS

Miocene sedimentary rocks (unit Ts; Plate 1) are locally exposed throughout the study area and are inferred to be more extensive in the subsurface (Fig. 9). On the basis of their present distribution, geometry, and lithology, we interpret these rocks to have been deposited in synextensional basins in the hanging walls of the major normal faults. In this section we describe the sedimentary rocks and their relationship to nearby structures at key localities. Dates from these deposits are from tephra correlations provided by Mike Perkins at the University of Utah (Table 2), and $^{40}Ar/^{39}Ar$ sanidine ages obtained at the U.S. Geological Survey (Tables 2 and 3). Table 2 summarizes all sample location, description, and age information, and Table 3 contains $^{40}Ar/^{39}Ar$ age data individual laser-fusion analysis. Tephra correlation methods were described by Perkins et al. (1998) and Perkins and Nash (2002). The $^{40}Ar/^{39}Ar$ analytical methods are described in Appendix A.

Description of the Miocene Sedimentary Rocks

Miocene sedimentary rocks in the study area weather white to pale brown and/or gray and commonly form conspicuous badlands topography, although actual outcrops are rare (Fig.

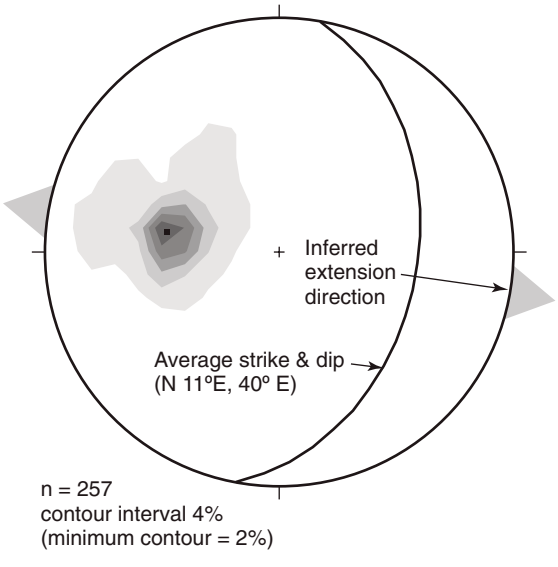

Figure 7. Lower hemisphere, equal-area plot of poles to bedding planes and compaction foliation from 35–25 Ma rocks within the Caetano caldera. Square is average pole of all measurements; great circle is plane to this pole (N11ºE, 40ºE). Gray arrows are inferred extension direction (N80ºW).

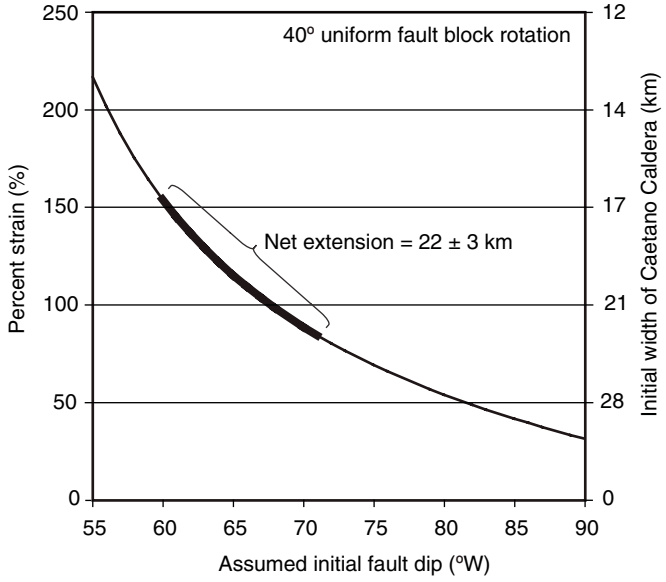

Figure 8. Plot of assumed initial fault dip versus percent strain (from equation 1) and resulting initial east-west width of the caldera, assuming 42 km present width. Range of probable initial fault dips (60º–70º; Table 1), yields 22 ± 3 km extension and an original east-west caldera width of ~20 km.

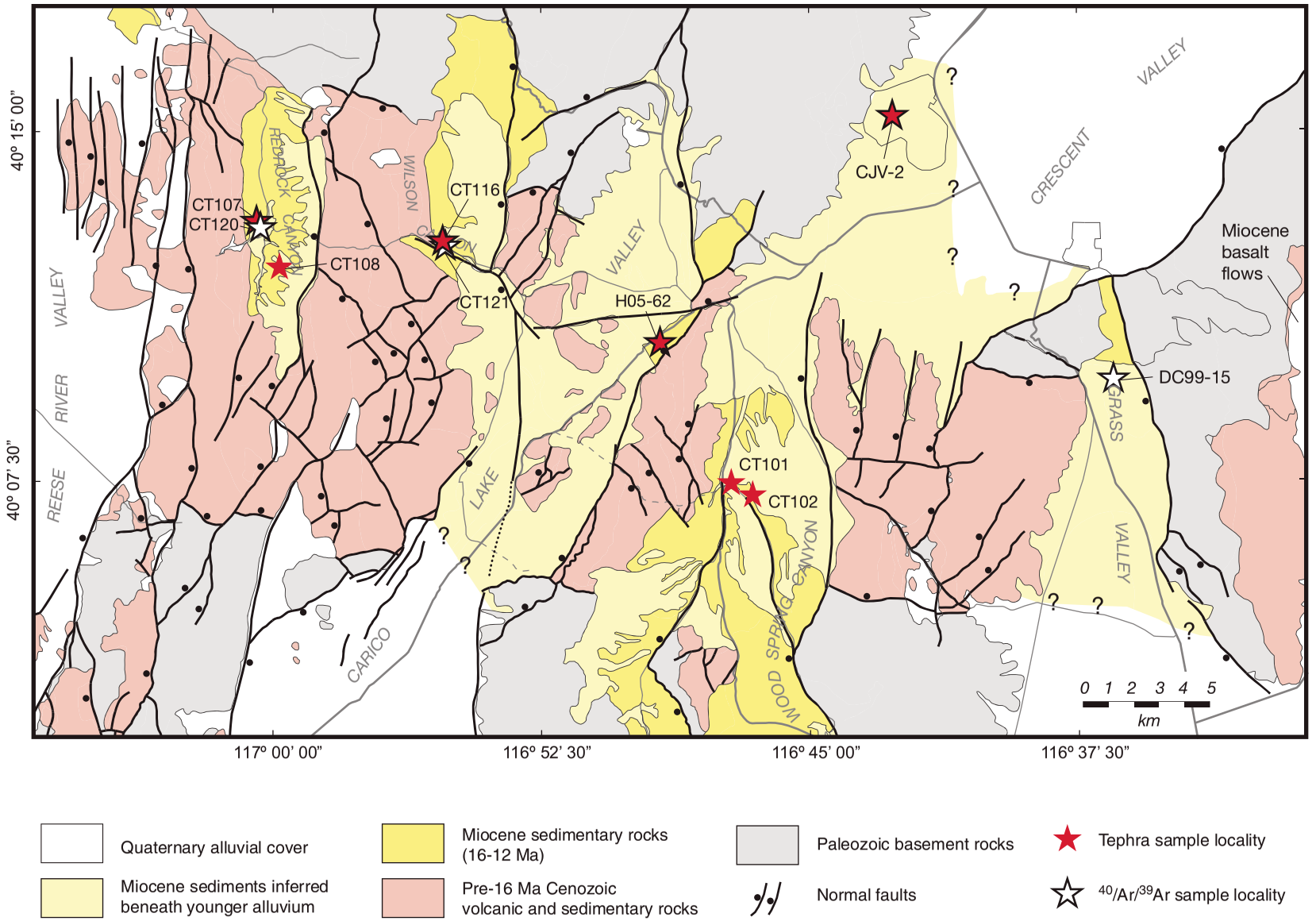

Figure 9. Map showing approximate extent of Miocene sedimentary rocks in the study area (same extent as Fig. 2 and Plate 1). Tephra correlations and $^{40}Ar/^{39}Ar$ data presented in Tables 2 and 3. Simplified from Plate 1.

TABLE 2. SAMPLE LOCATION AND AGE DATA FROM MIOCENE SEDIMENTARY ROCKS

Sample number	Latitude (°N)*	Longitude (°W)*	Sample description	Tephra correlation	Age (Ma)
JC06-CT107	40°13′04″	117°00′26″	Near base of section above Moss Creek canyon, conformable on unit C of Bates Mountain Tuff	Buffalo Canyon type, several matches in the 15.3–16 Ma interval	15.84 ± 0.15†
JC06-CT120	40°13′11″	117°00′23″	Near base of section above Moss Creek canyon, conformable on unit C of Bates Mountain Tuff	n/a	15.68 ± 0.14†
JC06-CT108	40°11′51″	116°59′53″	South-central Redrock Canyon, east of 4wd road south of Smith Flat	Cougar Point V	12.07‡
JC06-CT116	40°12′47″	116°55′19″	Base of section at south end of Wilson Canyon, conformable on unit D of Bates Mountain Tuff	Yellowstone hotspot tephra; several matches in the 13–15 Ma interval	15.38 ± 0.30†
JC06-CT121	40°12′46″	116°55′19″	Base of section at south end of Wilson Canyon, 25 ± 5 m upsection from CT116	n/a	15.03 ± 0.10†
H05-62	40°10′33″	116°49′00″	Hanging wall of Rocky Pass Fault, northern Carico Lake Valley	Twin Falls type Yellowstone hotspot tephra, several matches in the 8.5–10.5 and 10.5–15.25 Ma interval	15.21 ± 0.07†
JC06-CT101	40°07′28″	116°47′16″	Along creek east of Toiyabe Mine haul road, 0.5 km east of Tub Spring	Cougar Point III	12.69‡
JC06-CT102	40°07′26″	116°47′14″	20–30 m upsection from CT101	Cougar Point V	12.07‡
CJV2	40°14′59″	116°43′18″	Pipeline Mine	Buffalo Canyon type, several matches in the 15.3–16 Ma interval	15.88 ± 0.1§
DC99-15	40°09′28″	116°36′31″	From 334 m depth in drill hole west of Cortez Fault. Collected by Barrick Gold Corp.	n/a	15.24 ± 0.17†

*North American Datum of 1927.
†Sanidine $^{40}Ar/^{39}Ar$ age (this study; Table 3).
‡Age known from tephra correlation only (Perkins et al., 1998; Perkins and Nash, 2002).
§Sanidine $^{40}Ar/^{39}Ar$ age (John et al., 2008).

10A). They consist predominantly of light gray and/or brown, fine- to medium-grained sandstones in beds 10–20 cm thick, containing variable amounts of pyroclastic material, including glass shards and crystal and lithic fragments. Locally, the sandstones contain thin (~10–20 cm) lenticular beds of conglomerate, with 1–5 cm clasts of (variably) quartzite, chert, and volcanic rocks (Fig. 10B). Less commonly, the section contains thinly laminated (<1 cm) tuffaceous shales or siltstones. The most conspicuous layers in the Miocene basins consist of 2–5 m thick layers of silver-gray and white tephra (Fig. 10C) in 5-cm-thick to 1-m-thick beds that often consist of nearly pure volcanic glass shards. Tephra deposits are locally cross-bedded at the scale of 10–50 cm and mixed with coarser crystal and lithic fragments, which we interpret as evidence of local reworking. Tephra and sandstone layers are locally bioturbated and sometimes display conspicuous folds interpreted as soft-sediment deformation (Fig. 10C). We interpret the tuffaceous sandstones and shales to have been deposited in fluvial, lacustrine, and medial to distal alluvial-fan settings with frequent pyroclastic input, both from direct ash fall and material washing in from the surrounding highlands. Based on tephra correlations (this study; Table 2), the pyroclastic material was derived from eruptions in northern Nevada and southwestern Idaho (Perkins and Nash, 2002; Perkins et al., 1998) and does not represent local volcanic activity during deposition of the Miocene sedimentary rocks.

Coarser deposits of sandstone and conglomerate are also present in the Miocene basins, although they rarely crop out and generally form soft slopes covered with angular clasts weathering out of an unexposed matrix. These deposits are generally light brown– to yellowish-weathering, predominantly medium-grained but locally coarse-grained sandstones, often with a silty matrix. Bedding is commonly massive but is 10 cm to more than 2 m where observed. Sandstone layers contain angular to subangular clasts of Paleozoic quartzite, chert, and Cenozoic volcanic rocks. Clasts are typically 1–5 cm across, but locally exceed 50 cm. Clast abundance ranges from absent to >50%; where present, clasts are matrix supported and often coarsen crudely upward (Fig. 10D). We interpret these deposits to represent debris-flow and sheet-flood deposits formed on alluvial fans (e.g., Whipple and Dunne, 1992; Blair and McPherson, 1994; Sohn et al., 1999).

Miocene Basin at Redrock Canyon

In Redrock Canyon, Miocene sedimentary rocks overlie units C and D of the Bates Mountain Tuff with no apparent angular discordance. At the upper (east) end of Moss Creek Canyon, the base of the section consists of coarse sandstone and conglomerate dipping 42°E and overlying unit C (28.8 Ma) of the Bates Mountain Tuff. The basal conglomerate contains clasts of Paleozoic quartzite and Tertiary volcanic rocks (to 50 cm). The coarse deposits are only a few meters thick, and are overlain by as much as ~200 m of poorly exposed, thinly bedded, white tuffaceous shale. Overlying the shale, an ~20-m-thick sequence of ash-rich beds crops out for ~500 m along strike in a low ridge. Tephra beds are locally cross-bedded and chaotically folded by what we infer to be soft-sediment deformation (Fig. 10C). Sanidine from a layer of relatively pure, silver-gray volcanic glass in this sequence (sample CT107) yielded multi-grain laser fusion ages ranging from 26.30 to 15.73 Ma, indicating contamination by older feldspar grains. A weighted mean of the four youngest analyses gives an age of 15.84 ± 0.15 Ma (Table 3), but this should be considered a maximum age for the sample. This tephra

TABLE 3: $^{40}Ar/^{39}Ar$ MULTI-GRAIN LASER FUSION DATA

Sample: JC06-CT107, Sanidine Lat: 40°13′04″N Long: 117°00′26″W Irradiation: IRR248-74 J = 0.00258222

Run #	$^{40}Ar^*$ (mol/g)	% $^{40}Ar^*$	$^{40}Ar/^{39}Ar$	$^{37}Ar/^{39}Ar$	$^{36}Ar/^{39}Ar$	K/Ca	Cl/K	Age (Ma, ±1σ)
07L0139A	1.7560E-14	97.67	3.62101	0.17577	3.0223E-04	2.98482	3.4820E-05	*16.403 ± 0.091*
07L0139B	7.6808E-15	99.05	3.42888	0.44126	2.0667E-04	1.18874	7.7620E-05	15.757 ± 0.155
07L0139C	7.6383E-15	99.96	3.42996	0.23255	3.3127E-05	2.25592	1.8497E-05	15.905 ± 0.159
07L0139D	8.7976E-15	100.48	3.43022	0.39671	1.9276E-05	1.32227	5.4750E-05	15.990 ± 0.152
07L0139E	2.2615E-14	98.31	5.78449	0.17983	3.5260E-04	2.91742	–6.7412E-05	*26.303 ± 0.130*
07L0139F	1.0235E-14	96.55	3.51250	0.25146	4.4834E-04	2.08627	1.0151E-04	15.733 ± 0.136
					Weighted mean age (Ma, ±2σ)	MSWD = 0.56		15.84 ± 0.15

Sample: JC06-CT120, Sanidine Lat: 40°13′11″N Long: 117°00′23″W Irradiation: IRR248-75 J = 0.00257409

Run #	$^{40}Ar^*$ (mol/g)	% $^{40}Ar^*$	$^{40}Ar/^{39}Ar$	$^{37}Ar/^{39}Ar$	$^{36}Ar/^{39}Ar$	K/Ca	Cl/K	Age (Ma, ±1σ)
07L0140A	1.4590E-14	96.95	3.5422	0.3043	0.0004	1.7240	0.00008	15.881 ± 0.099
07L0140B	3.6577E-14	98.63	3.4359	0.2231	0.0002	2.3516	0.00007	15.671 ± 0.065
07L0140C	1.0274E-14	96.29	3.4550	0.3451	0.0005	1.5203	0.00002	15.387 ± 0.123
07L0140D	1.3657E-14	98.65	3.4487	0.2641	0.0002	1.9861	0.00008	15.733 ± 0.106
07L0140E	9.3218E-15	95.84	3.5593	0.5175	0.0006	1.0135	0.00003	15.777 ± 0.149
07L0140F	2.2573E-14	97.22	3.4750	0.2917	0.0004	1.7982	–0.00004	15.625 ± 0.077
					Weighted mean age (Ma, ±2σ)	MSWD = 2.2		15.68 ± 0.14

Sample: JC06-CT116, Sanidine Lat: 40°12′47″N Long: 116°55′19″W Irradiation: IRR248-77 J = 0.00255861

Run #	$^{40}Ar^*$ (mol/g)	% $^{40}Ar^*$	$^{40}Ar/^{39}Ar$	$^{37}Ar/^{39}Ar$	$^{36}Ar/^{39}Ar$	K/Ca	Cl/K	Age (Ma, ±1σ)
07L0141A	4.0836E-16	24.07	18.08233	1.32066	0.04667	0.39698	0.00421	*19.995 ± 4.613*
07L0141B	2.6366E-14	98.27	3.38961	0.01415	0.00017	37.07273	0.00024	15.31 ± 0.07
07L0141C	2.0738E-14	95.43	3.57297	0.21158	0.00058	2.47957	0.00017	15.672 ± 0.085
07L0141D	1.1063E-14	97.44	3.37713	0.08334	0.00029	6.29553	–0.00005	15.127 ± 0.124
07L0141E	7.5916E-15	98.07	3.44823	0.40856	0.00031	1.28393	0.00022	15.547 ± 0.171
07L0141F	8.7440E-15	93.61	3.50427	0.61603	0.00090	0.85139	0.00024	15.085 ± 0.147
					Weighted mean age (Ma, ±2σ)	MSWD = 5.5		15.38 ± 0.30

Sample: JC06-CT121, Sanidine Lat: 40°12′46″ Long: 116°55′19″W Irradiation: IRR248-69 J = 0.00269804

Run #	$^{40}Ar^*$ (mol/g)	% $^{40}Ar^*$	$^{40}Ar/^{39}Ar$	$^{37}Ar/^{39}Ar$	$^{36}Ar/^{39}Ar$	K/Ca	Cl/K	Age (Ma, ±1σ)
07L0137A	1.5757E-14	97.31	3.14519	0.05311	0.00027	9.87844	0.00006	14.836 ± 0.086
07L0137B	3.1625E-14	98.89	3.13990	0.04991	0.00010	10.51244	0.00007	15.051 ± 0.062
07L0137C	2.2742E-14	99.34	3.13362	0.10950	0.00007	4.79150	0.00004	15.089 ± 0.071
07L0137D	2.6799E-14	98.93	3.15222	0.04713	0.00010	11.13280	0.00007	15.117 ± 0.068
07L0137E	1.5024E-14	98.86	3.13788	0.14430	0.00013	3.63585	0.00000	15.038 ± 0.096
07L0137F	3.4150E-14	99.07	3.11904	0.04540	0.00008	11.55700	0.00007	14.979 ± 0.061
					Weighted mean age (Ma, ±2σ)	MSWD = 1.6		15.03 ± 0.10

Sample: H05-62, Sanidine Lat: 40°10′33″N Long: 116°49′00″W Irradiation: IRR248-72 J = 0.00259711

Run #	$^{40}Ar^*$ (mol/g)	% $^{40}Ar^*$	$^{40}Ar/^{39}Ar$	$^{37}Ar/^{39}Ar$	$^{36}Ar/^{39}Ar$	K/Ca	Cl/K	Age (Ma, ±1σ)
07K0144A	2.3889E-14	99.68	3.29102	0.04138	0.00002	12.67945	0.00002	15.306 ± 0.071
07K0144B	2.8473E-14	98.84	3.28079	0.05149	0.00011	10.19005	0.00001	15.130 ± 0.066
07K0144C	1.0790E-14	98.88	3.29489	0.18204	0.00015	2.88193	0.00006	15.203 ± 0.125
07K0144D	1.6677E-14	99.20	3.28283	0.19640	0.00011	2.67116	0.00001	15.197 ± 0.091
07K0144E	1.4710E-14	98.95	3.30401	0.05456	0.00010	9.61698	0.00010	15.254 ± 0.085
07K0144F	2.3652E-14	98.55	3.29878	0.10627	0.00016	4.93701	0.00001	15.169 ± 0.069
					Weighted mean age (Ma, ±2σ)	MSWD = 0.78		15.21 ± 0.07

Sample: DC99-15, Sanidine Lat: 40°09′28″N Long: 116°36′31″W Irradiation: IRR248-76 J = 0.00256571

Run #	$^{40}Ar^*$ (mol/g)	% $^{40}Ar^*$	$^{40}Ar/^{39}Ar$	$^{37}Ar/^{39}Ar$	$^{36}Ar/^{39}Ar$	K/Ca	Cl/K	Age (Ma, ±1σ)
07L0142A	5.5825E-15	99.09	3.33182	0.06231	0.00009	8.42091	0.00020	15.218 ± 0.215
07L0142B	1.5507E-14	99.09	3.33743	0.05085	0.00008	10.31831	0.00009	15.244 ± 0.094
07L0142C	3.1765E-14	81.07	8.61818	0.02899	0.00550	18.09819	0.00017	*32.055 ± 0.174*
07L0142D	6.4883E-15	99.45	3.75987	0.04101	0.00006	12.79120	0.00072	*17.225 ± 0.22*
07L0142E	1.7789E-14	98.36	3.52706	0.05090	0.00018	10.30823	0.00025	*15.988 ± 0.09*
07L0142F	6.3388E-15	77.16	5.39802	0.03815	0.00415	13.75560	0.09337	*19.177 ± 0.281*
					Weighted mean age (Ma, ±2σ)	MSWD = 0.91		15.24 ± 0.17

Note: Ages in italics excluded from weighted-mean age.

was independently correlated with 16.0–15.3 Ma Buffalo Canyon–type tephra (Table 2; Perkins and Nash, 2002). Sanidine from a second tephra sample in this sequence (sample CT120) yielded an age of 15.68 ± 0.14 Ma based on six reproducible multigrain laser fusion analyses (Table 3). From these dates, we conclude that deposition of the middle Miocene sedimentary rocks at Redrock Canyon began at or shortly before 15.8–15.6 Ma. Although we interpret the conglomerate and shale between the dated tephra horizon and the Bates Mountain Tuff to be middle Miocene (close to 16 Ma), it is important to note that geologic relationships permit it to be anywhere between 29 and 16 Ma.

To the south of Moss Creek Canyon, the base of the Miocene section overlies unit D (25.3 Ma) of the Bates Mountain Tuff (unit C is also present). Approximately 2 km southeast of Moss Creek, an isolated outcrop of relatively fresh white tephra (sample CT106; Fig. 9) was correlated with the 12.07 Ma Cougar Point V tuff (Table 2; Perkins and Nash, 2002). This exposure would be 600–700 m upsection from the Bates Mountain Tuff, although most of the intervening section is covered and we cannot rule out repetition by unexposed faults. Although the rest of the section to the east (upsection) is also covered by younger alluvium, we estimate at least 200–300 m of additional section above the ca. 12 Ma tephra. From this date, we conclude that deposition in the Redrock Canyon basin continued up to and after 12 Ma. The low hills on the east (fault bound) side of Redrock Canyon consist of soft, sandy and silty soil weathering out small (<10 cm) angular chips of tuff and Paleozoic quartzite. We interpret these deposits as poorly consolidated conglomerate within the Miocene sedimentary section, but we have not observed any actual outcrops. These deposits are concealed and truncated by a pediment surface covered with large (up to several meters) boulders of Caetano Tuff presumably derived from the adjacent highlands.

Miocene Basin at Wilson Canyon

At the mouth of Wilson Canyon, 40°E dipping tuffaceous sandstones with interbedded tephra layers conformably overlie unit D (25.3 Ma) of the Bates Mountain Tuff. Sanidine from a prominent, white, thinly bedded (~2 cm), 1-m-thick layer of tephra ~10 m above the Bates Mountain Tuff (sample CT116; Fig. 9) yielded multigrain laser-fusion $^{40}Ar/^{39}Ar$ ages ranging from 15.09 ± 0.05 to 20.0 ± 4.6 Ma (Table 3), indicating contamination by older feldspar grains. Excluding the 20 Ma date and calculating a weighted mean of the remaining five multigrain analyses (15.67–15.09 Ma; Table 3) yields an age of 15.38 ± 0.30 Ma, although the eruptive age may be as young as 15.09 Ma. This sample was independently correlated with any of several Yellowstone hotspot–type tephras ranging in age from 13 to 15 Ma (Table 2; Perkins and Nash, 2002). Upsection from this tephra bed, the section grades to tan, medium-grained sandstone in beds 20–150 cm thick, with a silty matrix and local small lenticular conglomerate beds (Fig. 10B). Sanidine from a tephra layer interbedded with these sandstones (sample CT121) yielded an $^{40}Ar/^{39}Ar$ age of 15.03 ± 0.10 Ma (Table 3) from the weighted mean of six reproducible multigrain laser-fusion analyses. From these dates, we conclude that deposition of the middle Miocene sedimentary rocks at Wilson Canyon began ca. 15.4–15.0 Ma, after a 10 m.y. hiatus following deposition of the Bates Mountain Tuff.

Much of the remaining section to the east is covered by younger alluvium at the northwest end of Carico Lake Valley, but a small sandstone outcrop 1.5 km to the southeast (an unknown distance upsection) dips 18°E. On the east side of this basin, along the haul road to the Greystone Mine, sandstone and conglomerate are exposed in roadcuts in the hanging wall of the Greystone fault, locally in direct contact with the fault (Fig. 5B). Although much of the section is covered by younger alluvium, we estimate it to be >1 km thick, assuming no repetition by unmapped faults.

Miocene Basin at Wood Spring Canyon

The most extensive and best-exposed (relative to the others) Miocene basin occupies the hanging wall of the Toiyabe Mine fault, between the Rocky Pass–Red Mountain block and the northern Toiyabe Range (Fig. 9). In the west-central part of the basin, east of Tub Spring, tuffaceous sandstones and shales (Ts) are mostly covered by a thin layer of younger alluvium (shown as Qaf in Plate 1). These units dip 20°–5°E where they are exposed in modern drainages (Fig. 10A). Two samples from this section (CT101 and CT102; Fig. 9) were correlated with the Cougar Point III (12.69 Ma) and Cougar Point V (12.07 Ma) tephras, respectively (Table 2; Perkins and Nash, 2002). The section is cut by at least one small fault (Plate 1) that appears to offset the ground surface as much as 100 m and is therefore assumed to be young (Pleistocene?), with essentially no displacement at the scale of cross section C–C' (Fig. 4). Assuming the section is not repeated by additional unmapped faults, ~300–400 m of section probably overlies the 12 Ma tephra layer. Much of it is covered by younger alluvium, but on the east side of the basin, close to the Toiyabe Mine fault, fine-grained tuffaceous sandstones and shales are overlain by medium- to coarse-grained, silty sandstones with uncommon matrix-supported clasts of Paleozoic quartzite. From the above dates, we conclude that deposition of the middle Miocene sedimentary rocks at Wood Spring Canyon continued up to and after 12 Ma.

The southwestern part of the basin, in the hanging wall of the Dry Canyon fault, consists primarily of gently east dipping (~12°) tuffaceous sandstone and shale, with the base of the section largely obscured by younger alluvium. Just west of the Dry Canyon fault, the basin contains coarse sandstone and conglomerate with subangular clasts of greenish Paleozoic chert (>80% of clasts), quartzite, and (presumably Cenozoic) volcanic rocks (to ~50 cm). The chert clasts are probably derived from similar-looking Paleozoic chert in the footwall of the Dry Canyon fault exposed <100 m to the east. These deposits are locally calcite cemented and crop out in highly resistant ledges, which we interpret as fossil spring deposits.

The southeast part of the basin, adjacent to the Toiyabe Mine fault, appears to consist primarily of medium-grained sandstone with a silty matrix, with varying amounts of matrix-supported angular Paleozoic chert and (predominantly) quartzite clasts (Fig. 10D). Outcrops of this deposit are very rare, but where exposed they exhibit poorly developed 50–150 cm bedding that dips gently (<10°) northeast. These deposits form a range of deeply dissected hills that rise to 7250 ft (2210 m) west of the Toiyabe Mine, and we estimate the section to be at least 1 km thick, with an unknown, but probably significant, thickness removed by erosion. The Toiyabe Mine fault occupies a deep canyon (200–300 m) between Paleozoic footwall rocks and hanging-wall basin sediments (Plate 1). The base of this section appears to (along D–D') overlie Bates Mountain Tuff (units C and D), but it is unclear whether the bulk of the overlying deposits is older or younger than the 12 Ma tuffs in the central part of the basin 5 km to the north (along C–C'). Although the deposits west of Toiyabe Mine are now topographically more prominent than the northern part of the basin, they dip gently northeast and may project under the 12 Ma tuffs to the north.

Other Miocene Basin Exposures

Several other exposures of Miocene sedimentary rocks in the study area yielded useful age constraints, although they are not from sections as complete or extensive as those described above. Along the east side of Carico Lake Valley, ~2 km southwest of Rocky Pass, fine-grained tuffaceous sandstones dip 24°E in the

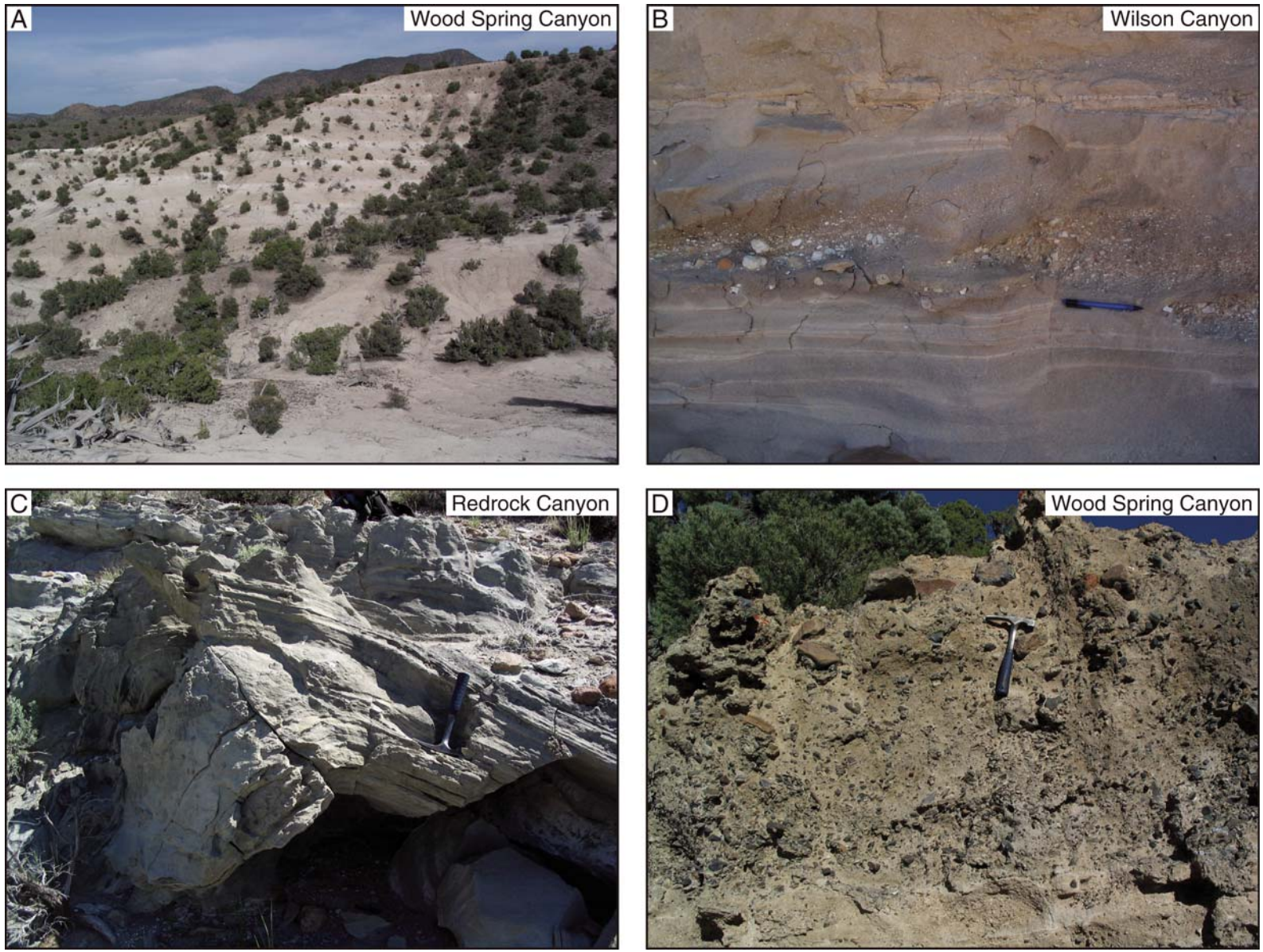

Figure 10. (A) Silty sandstone packages (each roughly 5 m thick) in the hanging wall of the Toiyabe Mine fault, lower Wood Spring Canyon. (B) Miocene sandstone beds, lower Wilson Canyon. Tephra interbedded with these deposits yielded an $^{40}Ar/^{39}Ar$ age of 15.03 ± 0.10 Ma (Tables 2 and 3). Pencil is 14 cm. (C) Folded tephra beds in Miocene sedimentary rocks east of Moss Creek Canyon with $^{40}Ar/^{39}Ar$ ages of 15.84 ± 0.15 Ma and 15.68 ± 0.14 Ma (Tables 2 and 3). (D) Matrix-supported angular conglomerate in the hanging wall of the Toiyabe Mine fault. Note crude inverse grading. Clasts are predominantly Paleozoic quartzite. Hammer in C and D is 27 cm.

hanging wall of the Rocky Pass fault. Sanidine from a tephra interbedded with these sandstones yielded an $^{40}Ar/^{39}Ar$ age of 15.21 ± 0.07 Ma, from a weighted mean of six reproducible multigrain laser-fusion analyses (sample H05–62; Fig. 9). This tephra was independently correlated with Twin Falls–type Yellowstone hotspot tephra, with a possible age ranging from 13 to 15.3 Ma (Table 2; Perkins and Nash, 2002).

Barrick Gold Corporation provided a tephra sample from a drill hole in the hanging wall of the Cortez fault (sample DC99–15; Fig. 9). Sanidine from this tephra yielded multigrain laser-fusion ages ranging from 32.1 to 15.2 Ma, indicating significant contamination by older feldspar grains. The two youngest analyses give a weighted mean age of 15.24 ± 0.17 Ma, and we consider this the best estimate for the age of the sample, although it may be slightly younger. We infer that the conglomerates and sandstones exposed in the footwall of the Crescent fault 4 km to the north (Fig. 6A) are correlative with the sedimentary rocks in this drill hole.

An additional sample was collected from exposures in the pit wall at the Pipeline Mine, where Miocene sedimentary rocks are deposited on lower-plate Paleozoic basement. Sanidine from a tephra within these deposits (sample CJV2; Fig. 9) yielded an $^{40}Ar/^{39}Ar$ age of 15.88 ± 0.10 Ma (John et al., 2008), and the same sample was independently correlated with 16.0–15.3 Ma Buffalo Canyon–type tephra (Table 2; Perkins and Nash, 2002).

Miocene Basins: Interpretation

From the geologic relationships and age data discussed above, we infer that Miocene sedimentation across the study area began at or shortly before 16–15 Ma, at which time the underlying 25–35 Ma volcanic and sedimentary rocks were essentially flat lying. With the exception of the paleovalley in the southern Cortez Range (John et al., 2008), pre–middle Miocene Cenozoic sedimentary rocks in the study area are older than 25 Ma and are confined to the topographic depression left by the Caetano caldera (Fig. 9). The absence of 25–16 Ma rocks in the study area suggests a period of tectonic quiescence, consistent with the presence of a low-relief land surface incised by paleovalleys, possibly with external drainage to the west (e.g., Henry, 2008; Gonsior and Dilles, 2008; John et al., 2008). In contrast to older sedimentary rocks, the middle Miocene (younger than 16 Ma) sedimentary rocks are confined to north-south elongate basins bound by north-striking normal faults. With the exception of the Redrock Canyon basin, the Miocene basins and north-striking normal faults cut directly across the old caldera margin (Fig. 9). We interpret this pattern to be strong evidence that the onset of the extensional faulting that dismembered the Caetano caldera was coeval with the onset of basin sedimentation at 16 Ma. Extensional faulting created accommodation space for the basins, supplied them with sediment from the eroding footwall blocks, and cut off any external drainage system that may have existed prior to 16 Ma.

Coarser deposits (conglomerate and sandstone) in Redrock Canyon, Wood Spring (Fig. 10D), and Wilson Canyons (Fig. 5B) (the best-preserved basins) appear to be concentrated on the east (fault bound) sides of the basins. Because rocks in these basins currently dip east, the coarser deposits are also the youngest exposures, so it is unclear whether this distribution represents upward coarsening related to changes in the rate of erosion and/or fault slip, or merely an oblique traverse across a lateral facies change that persisted for the lifetime of the basin. Where exposed at Wilson and Moss Creek Canyons, there is no significant angular unconformity between the base of the Miocene sedimentary section and the underlying Oligocene tuffs, and the dip of the overlying Miocene deposits appears to shallow upsection to the east (Plate 1). The base of the Miocene section at Wood Spring Canyon has not been mapped, but the dip of the exposed part of the section decreases eastward (upsection) from ~20° to <10°, while the underlying Caetano Tuff dips ~40°E. This geometry is consistent with deposition during fault slip and tilting of the basins, although some component of tilting may be caused by unmapped intrabasin faults or tilting of the entire basin (and its bounding fault) by a younger generation of faults. Overall, however, the distribution and geometry of the Miocene sedimentary rocks are consistent with deposition in small (2–3 km across), active half-graben basins, with the coarser material deposited adjacent to the bounding faults, and lower-energy deposits in the distal part of the basins (e.g., Leeder and Gawthorpe, 1987).

The style of faulting and sedimentation in the study area appears more analogous to the supradetachment basins developed over and around metamorphic core complexes than to the wide (20–30 km across), gently tilted (<10°) half-graben basins forming in Nevada today. Sedimentation in supradetachment systems often begins in a single broad basin and becomes confined to narrow, rapidly tilting half-grabens as faulting progresses, and the basins are often broken up by numerous faults (e.g., Dickinson, 1991; Miller and John, 1999; McClaughry and Gaylord, 2005). Middle Miocene sedimentary rocks in our study area are currently restricted to discrete basins, but it is possible that they were originally more extensive and have been removed by erosion. We have not mapped any significant faults within the basins, although more detailed mapping may reveal some, particularly in the Wood Spring Canyon basin. Overall, although the basin geometry is similar, the structure of our study area is considerably simpler than true supradetachment basins, probably due to less extreme strain, which was not sufficient to exhume the mid-crustal underpinnings of the extended area.

We consider the simplest interpretation of the observed distribution, geometry, and age of the Miocene sedimentary rocks to be deposition in synextensional basins that formed in response to slip on the major normal faults that dismembered the Caetano caldera. Deposition appears to have begun across the study area at or shortly before 16–15 Ma and continued, at least locally, until sometime more recently than 12 Ma. Middle Miocene sedimentary rocks similar to those described in this study crop out across much of northeastern Nevada (Stewart and Carlson, 1978), where they are assigned to the Humboldt Formation (Sharp, 1939; Smith and Ketner, 1976, Wallace et al., 2008) and the informal Carlin formation (Regnier, 1960). These formations range from 16 to 15 Ma to ca. 10 Ma (Smith and Ketner, 1976; Perkins and Nash, 2002; Wallace et al., 2008), and therefore we suggest a similar 10 Ma upper age limit for the Miocene basins described in this study.

DISCUSSION AND CONCLUSIONS

Timing and Structural Style of Extension

Lack of Evidence for Pre-Miocene Extension

The lack of angular discordance between 34 and 25 Ma deposits within the Caetano caldera demonstrates that no significant deformation took place in the study area over that interval, aside from local doming related to magma resurgence within the caldera (Fig. 11A). Very few Cenozoic rocks in the study area predate the Caetano caldera, and those that do are small-volume lava flows and gravels that appear to fill <1 km of paleotopography in the southern Cortez Range (John et al., 2008). Where related rocks crop out on the caldera floor near Wenban Spring (Fig. 2), they are conformable with the overlying Caetano Tuff (John et al., 2008). Given the lack of direct evidence for Eocene or older extension (in the form of faults, angular unconformities, or sedimentary basins), we conclude that the study area underwent essentially no Cenozoic deformation prior to the onset of extension in the middle Miocene. The absence of any units in the 25–16 Ma interval is consistent with low relief and external drainage such

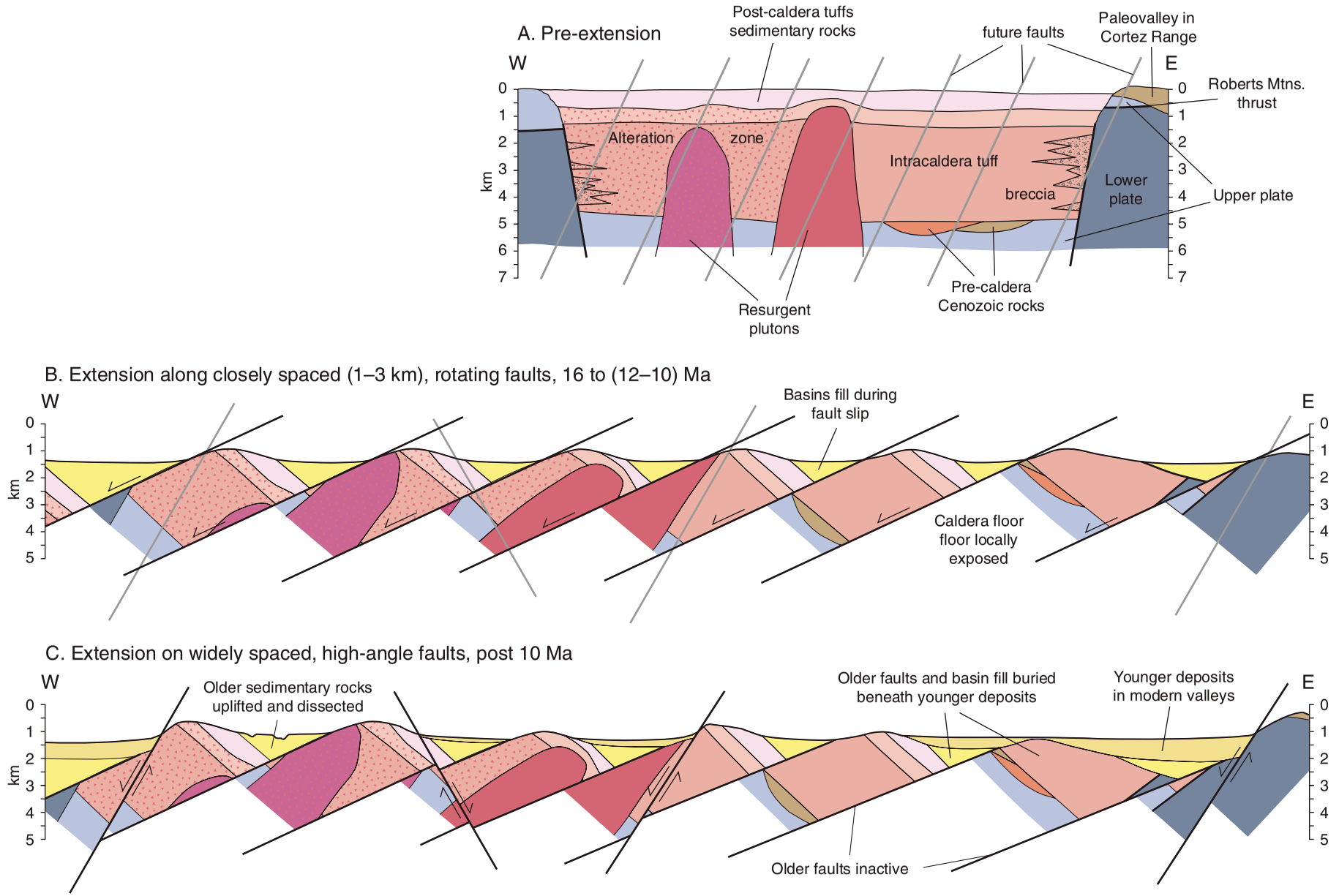

Figure 11. Illustration of Miocene extension of the Caetano caldera. Sections are east-west through the center of the caldera. No vertical exaggeration. (A) Pre-extensional Caetano caldera, modified from Figure 20D of John et al. (2008). (B) Middle Miocene extension on closely spaced, domino-style normal faults, with sedimentation in small half-graben basins. (C) Widely spaced, high-angle normal faulting with broad sedimentary basins.

as the paleovalleys documented in nearby areas (John et al., 2008; Gonsior and Dilles, 2008; Henry, 2008).

Large-Magnitude Middle Miocene Extension

Middle Miocene extension was accommodated by initially high angle (≥60°), closely spaced (1–3 km) faults that underwent significant rotation during fault slip (Fig. 11B). Although these faults are cut by younger faults, the younger faults appear to represent a distinct, more recent period of faulting with a different regional stress field (e.g., Zoback et al., 1994), rather than successive generations of crosscutting normal faults formed during progressive footwall rotation (e.g., Proffett, 1977; Miller et al., 1983). Given the poor exposure of faults and the difficulty of tracing them through intracaldera tuff and Paleozoic basement, however, it is possible that we are simply unable to distinguish crosscutting faults formed very closely in time and space. Likewise there are few subsurface data that bear on the geometry of these faults at depth. The simplest interpretation is that faults mapped at the surface originally merged downward into a brittle-ductile transition zone, beneath which extension was accommodated by ductile flow (e.g., Gans, 1987). Regardless of precisely how the strain was accommodated in the subsurface, it is clear that the upper crust in the study area underwent significant (~100% strain) extension.

Based on our interpretation of the middle Miocene synextensional basins, we conclude that this faulting began at or shortly before 16 Ma, but the rate and duration of subsequent extension are more difficult to determine. The 12 Ma tephra layers in the Redrock Canyon and Wood Spring basins are east tilted, consistent with some tilting—and presumably faulting—after this time. Continued slip on the Miocene basin-bounding normal faults after 12 Ma is consistent with ongoing deposition in the adjacent basins (above the 12 Ma tephras), which may be as young as 10 Ma. Alternatively, entire basins, together with their bounding faults and footwalls, may have been tilted somewhat by later slip on a younger generation of normal faults (discussed below), although even the largest of these faults appear to tilt nearby rocks only 6°–7°. At present, the simplest conclusion is that extension of the Caetano caldera began ca. 16 Ma and slip on the major faults continued until as recently as 10 Ma, although faulting need not have proceeded at a constant rate over that interval, nor at exactly the same time and/or rate in each individual basin. Apatite fission-track and (U-Th)/He data from the nearby East Range (Fig. 1) document rapid exhumation and fault slip ca. 17–15 Ma (Fosdick et al., 2006), providing somewhat independent evidence for middle Miocene extension in this part of Nevada.

Late Miocene and Younger Extension

Gently dipping faults, tilted footwall blocks, and hanging-wall basins formed during middle Miocene extension were subsequently cut by younger faults and are now exhumed to varying degrees in the footwalls of these faults (Fig. 11C). This is most spectacularly evident at the Cortez Mine (Fig. 2), where the Crescent fault (Fig. 6A) cuts the Cortez fault and its hanging-wall basin at a right angle, exposing it in cross section. It is these younger, more widely spaced (20–30 km) faults that are responsible for the modern topography of the basins and ranges in the study area. Although they accommodate relatively little horizontal extension, these faults dip steeply (50°–60°) and some have significant vertical offset (2–3 km), forming large, deep basins (e.g., Crescent and Reese River Valleys; Fig. 2). They strike more northeast than the older, middle Miocene faults, particularly in the vicinity of the northern Nevada Rift (Fig. 1). Several of these faults have evidence for Holocene offset, including the Crescent fault (Friedrich et al., 2004), and the faults bounding the Shoshone Range to the west and north (Wesnousky et al., 2005). Several faults documented in this study may have Holocene displacement, notably the Red Mountain fault (Fig. 6C) and additional faults on the west side of Carico Lake Valley (Plate 1).

The onset of this faulting is more difficult to determine. Regionally, it must postdate ca. 15 Ma basalt flows on the crest of the Shoshone and Cortez Ranges (Fig. 1; Armstrong, 1970; John et al., 2000). In the study area, a significant part of it must postdate the youngest dated Miocene sedimentary rocks (at least 12 Ma, and possibly 10 Ma) that have been uplifted relative to the modern valley floors. Present-day slip rates for Basin and Range normal faults are on the order of 0.2–0.4 mm/yr (e.g., Bennett et al., 2003; Niemi et al., 2004); if these are indicative of long-term rates, then the largest of the late Miocene faults must have been active for millions of years. This is supported by apatite (U-Th)/He ages as young as 9–10 Ma from the Cortez Range (Fig. 1; Colgan and Metcalf, 2006) and the East Range (Fig. 1; Fosdick et al., 2006), which require significant (>2 km) exhumation since that time, although in both cases, faulting may have begun more recently. It is therefore unclear at present whether there was a significant time lag in central Nevada between the end of large-magnitude middle Miocene extension and the onset of modern Basin and Range extension, or if there was a continuous transition between these two different styles of deformation.

Extension of Areas Surrounding the Caetano Caldera

Given significant (100% or more) extensional strain documented across the Caetano caldera, how far does this style and magnitude of deformation extend along strike into nearby areas? For Miocene extension to have been confined to the caldera, the caldera margin would need to have functioned as a strike-slip accommodation zone with kilometers of offset (e.g., Faulds and Varga, 1998). Detailed mapping of the caldera margin at Wilson Pass, Elephant Head, Red Mountain, and the northern Toiyabe Range (Plate 1; Fig. 2) reveals no evidence for significant strike-slip faulting (John et al., 2008). Muntean et al. (2001) also examined the caldera margin in the Shoshone Range and came to the same conclusion, although they did not interpret the boundary as a caldera margin. Everywhere it is exposed, the caldera margin appears to be a high-angle fault or buttress unconformity that juxtaposes intracaldera tuff and breccia with Paleozoic wall rocks, all of which are east tilted by later normal faults (this study; John et al., 2008). Even if the caldera margin were a large-offset strike-slip fault, that deformation would have to predate the Miocene normal faults and basins that demonstrably cut the caldera margin, requiring extension have taken place on an earlier (pre–16 Ma) set of faults and/or basins that left no trace in the geologic record. Therefore, it seems almost certain that large-magnitude extension is not confined to the caldera. In the following section, we examine evidence for late Cenozoic extension of the areas immediately south (section D–D'; Plate 1) and north of the caldera (Toiyabe and Shoshone Ranges).

Late Cenozoic Extension South of the Caetano Caldera (Section D–D')

Many of the major faults and Miocene extension basins mapped within the Caetano caldera can be shown to continue along strike to the south, cutting the caldera margin and adjacent wall rocks (Plate 1). The lack of reliable Cenozoic marker units and complex deformation of Paleozoic basement rocks make it impractical to restore cross section D–D', but it highlights locations where deformation (faulting and tilting) of the caldera can be shown to continue into surrounding Paleozoic rocks.

The western part of D–D' crosses the Cedars area (Fig. 2) in the southern Shoshone Range, mapped in detail (scale 1:24,000) by Moore et al. (2005). At this latitude, the Shoshone Range is a horst block, bound to the west by the southern extension of the Moss Creek fault system and to the east by the Stone Cabin fault. Internally, the range is split by the north-striking Cedars fault,

which dips ~40°W where exposed in the central part of the range. The Cedars fault drops upper Paleozoic Overlap assemblage (Pzo) overlain by ca. 34 Ma dacite lava flows (Tad) down against siliceous upper-plate lower Paleozoic rocks (Moore et al., 2005). At least 1.5–2.0 km of slip is required to restore the overlap sequence in the hanging wall of the Cedars fault above the lower plate in the footwall. To the east, upper-plate rocks in the footwall of the Cedars fault are cut by the west-dipping Elephant Head fault, which was inferred by Moore et al. (2005) to die out southward and merge with (or be cut by) the Cedars fault just north of section D–D'. Both the Cedars and Elephant Head faults clearly cut the caldera margin in the southern Shoshone Range (this study; Moore et al., 2005). We suggest that the upper Paleozoic Overlap assemblage and overlying Cenozoic rocks (Tad and Tct?) that must once have overlain upper-plate rocks in the footwall of the Cedars fault are now buried beneath alluvium in Carico Lake Valley, although there are no subsurface data to confirm this interpretation.

On the east side of Carico Lake Valley, upper-plate Paleozoic quartzite and chert are exposed at Red Mountain in the footwall of a west-dipping normal fault. Where the caldera margin is exposed just north of Red Mountain, intracaldera Caetano Tuff dips 30°–40°E and is cut by an ~40°W dipping fault observed to cut south across the caldera margin and into surrounding rocks. It is unclear, however, if the fault bounding Red Mountain to the west along D–D' is part of the Rocky Pass or Greystone fault systems, or if the fault is related to the younger Red Mountain fault (Fig. 6C) that cuts older faults and appears to have undergone late Quaternary slip. In either case, it is clear that Paleozoic rocks at Red Mountain have been exhumed and east tilted in the footwall of the same fault system that exhumed the Caetano caldera 2.5 km to the north.

Between Red Mountain and the Toiyabe Mine, upper-plate rocks exposed in the footwall of the Dry Canyon fault are overlain unconformably by outflow Caetano Tuff and Bates Mountain Tuff. The Cenozoic tuffs generally dip east (~25°–35°), but are locally complicated by several small faults and anomalous west dips in the Bates Mountain Tuff. The footwall of the Dry Canyon fault is surrounded by Miocene sedimentary rocks (Ts), and it is unclear if or how the Dry Canyon fault continues north through or beneath the basin. The lack of Cenozoic rocks on the east side of Red Mountain makes restoring this fault difficult, but along D–D' the Dry Canyon fault appears to have 2–3 km of slip.

The Toiyabe Mine fault cuts the southern margin of the caldera (the Wenban fault of Gilluly and Masursky, 1965) and is named for the Toiyabe Mine along section D–D'. Here, the Toiyabe Mine fault drops Miocene sandstone and conglomerate (Ts) down against Paleozoic rocks. The fault now occupies a deep canyon separating hanging-wall sedimentary rocks from footwall Paleozoic rocks. With the exception of lower-plate rocks near the Toiyabe Mine, the footwall of the Toiyabe Mine fault along D–D' exposes only upper-plate rocks across the width of the Toiyabe Range, and it is unclear if or where the Caetano Ranch fault continues to the south across the caldera margin. If the Toiyabe Range along D–D' was intact and tilted 40º–60ºE like the intracaldera tuff to the north, the upper plate would be >5 km thick, which seems unreasonable given its documented 1–2 km thickness elsewhere in and around the study area (this study; Gilluly and Masursky, 1965; Gilluly and Gates, 1965). Therefore, we believe it likely that the Caetano Ranch fault cuts the southern caldera margin and repeats the upper-plate rocks in the northern Toiyabe Range.

Late Cenozoic Extension North of the Caetano Caldera

Toiyabe Range. The northeastern margin of the caldera in the Toiyabe Range (the Copper fault of Gilluly and Masursky, 1965) is the best-preserved and most laterally continuous (4 vertical km) exposure of the caldera margin (John et al., 2008). South of this caldera margin, intracaldera tuff and breccia deposits dip ~40ºE (section B–B'; Fig. 4; Plate 1). We infer that tilting of the tuff resulted from slip on the Caetano Ranch fault, which was later cut at an oblique angle by the younger Crescent fault. Because there is no evidence for structural decoupling of the Caetano caldera from the Paleozoic rocks north of the caldera margin in the Toiyabe Range, it follows that the Paleozoic rocks (and associated mineral deposits) in and around the Cortez mine (Fig. 2) were also east tilted during Miocene extension.

To the north of the Toiyabe Range, the margin of the Caetano caldera is covered by alluvium at the south end of Crescent Valley, and it is unclear if or how the major faults mapped within the caldera continue along strike to the north. Given the significant displacement on the Toiyabe Mine and Caetano Ranch faults along section B–B', we consider it likely that they continue at least some distance north beneath Crescent Valley. They are shown schematically on section A–A' as they would project from exposures along B–B', although we have no subsurface data to confirm this interpretation. If the extended area continues 9–10 km north of A–A' (Plate 1), it is possible that the Pipeline deposit (Fig. 2) has been displaced several kilometers westward from its original location.

Shoshone Range. The northern Shoshone Range (Fig. 1) exposes a large expanse of highly deformed Paleozoic rocks in the upper plate of the Roberts Mountains allochthon, punctuated by rare lower-plate windows, numerous Tertiary intrusions, and isolated outcrops of Tertiary volcanic rocks (Gilluly and Gates, 1965). The northern caldera margin is not widely exposed in the Shoshone Range, and no pre–16 Ma Cenozoic rocks are exposed within our study area that would provide a marker for late Cenozoic extension north of the caldera (Plate 1). However, given significant extension of the caldera just south of the margin (western part of A–A'; Fig. 4), together with the lack of evidence for significant strike-slip displacement along the caldera margin, we consider it likely that the Shoshone Range in the northern part of our study area (Plate 1) was extended together with the adjacent caldera. Muntean et al. (2001) raised the possibility of significant extension in the Shoshone Range, but proposed that deformation was localized along a detachment fault at the base of the Tertiary and that the Paleozoic basement was relatively little deformed by normal faults. Here, we propose that the Shoshone Range (at least within a few kilometers of the northern caldera margin) was extended along the same set of west-dipping, initially high-angle normal faults that dismembered the Caetano caldera to the south.

The Greystone fault cuts the caldera margin along A–A' (Fig. 4; Plate 1) and continues north for at least 7 km into the Shoshone Range, where it is exposed in several roadcuts (Fig. 5B). The caldera margin here juxtaposes 40°–60°E dipping intracaldera tuff and breccia with Paleozoic wall rocks and is cut by a small ring-fracture intrusion (John et al., 2008). We have found no evidence for strike-slip faulting along the caldera margin, so presumably the Paleozoic rocks immediately north of the caldera margin are also east tilted. Miocene sedimentary rocks exposed east of Wilson Canyon in the hanging wall of the Greystone fault also strike north across the caldera margin, consistent with Miocene extensional faults cutting the caldera margin and extending at least 7–8 km north into the Shoshone Range.

The Redrock Canyon fault has ~6 km of slip along section A–A' (Fig. 4), <4 km south of caldera margin in the western Shoshone Range (Plate 1). Slip on this fault does not appear to diminish significantly to the north and was sufficient to expose the caldera floor only a few hundred meters south of the caldera margin west of Wilson Pass (Plate 1). Only a few hundred meters north of the caldera margin, lower-plate rocks are exposed beneath the Robert Mountains thrust on the west side of Horse Mountain

(Plate 1). Gilluly and Gates (1965) mapped this lower-plate window as the core of an anticline, with the Roberts Mountains thrust and overlying upper plate dipping east and west away from Horse Mountain. We suggest instead that lower-plate rocks at Horse Mountain are exposed in the footwall of the Redrock Canyon fault, which cuts the caldera margin and strikes north into the Shoshone Range. In this interpretation, the western "thrust" contact between upper and lower-plate rocks at Horse Mountain would actually be a down-to-the-west normal fault. This fault contact is about 1 km north along strike from the mapped trace of the Redrock Canyon fault within the caldera, although the exact point where the fault would cut the caldera margin is covered by colluvium (Plate 1). Although we have not mapped the Tertiary rocks north of the caldera margin (north of Plate 1), we have observed the tuff of Cove Mine and another tuff (probably unit B of the Bates Mountain Tuff) dipping 35°–60°E at the mouth of Harry Canyon (~6 km north of caldera margin), consistent with Miocene extension and tilting of the Shoshone Range north of the Caetano caldera.

Extension and the Northern Nevada Rift

The northern Nevada rift is a prominent north-northwest–trending magnetic anomaly in central Nevada that coincides in part with a zone of mafic dikes and lava flows at the surface (Fig. 1; e.g., Zoback et al., 1994). The rift formed between ca. 16.5 and 15 Ma, coeval with the widespread middle Miocene magmatic episode that produced the Columbia River Basalts and similar rocks in Washington, Oregon, and northwestern Nevada (e.g., Zoback et al., 1994; John et al., 2000). Structurally, the rift is a 5–15-km-wide zone bound by high-angle faults and filled with ~500 m (locally >1 km) of mafic lava flows and minor sedimentary rocks. A 3–5-km-wide zone of mafic dikes intrudes basement rocks and Miocene volcanic rocks within the rift zone (John et al., 2000). The rift is currently broken by north- to northeast-striking, late Miocene (?) and younger normal and oblique-slip faults, but it was formed along the western edge of a middle Miocene stable (unextended) block that included the modern Cortez Range (Fig. 1). The orientation of the rift is thought to reflect a Basin and Range–wide middle Miocene extension direction oriented ~N70°E (Zoback and Thompson, 1978; Zoback et al., 1994).

The oldest dates from Miocene sedimentary basins within our study area are 15.0–15.6 Ma—within the age range of northern Nevada rift mafic dikes and lava flows in the nearby Shoshone and Cortez Ranges (Fig. 1) (16.8–15.0 Ma; John et al., 2000). If we are correct that these basins formed contemporaneously with extensional faulting, then extension of the Caetano caldera began shortly after inception of the northern Nevada rift at 16.5 Ma, and initial extension was contemporaneous with emplacement of nearby rift dikes. Based on the tilting of intracaldera tuffs and sedimentary rocks (Fig. 7), we infer that extension of the Caetano caldera was oriented ~N80°W, or ~30° different than the extension direction inferred from the northern Nevada rift (N65°–70°E; Zoback et al., 1994). Either the regional shift from extension oriented ~N70°E (the rift direction) to ~N70°W (the modern direction; Zoback et al., 1994) took place during the later stages of rift magmatism (ca. 15.5 Ma or later), or the rift does not truly reflect the regional middle Miocene extension direction across the northern Basin and Range. A number of workers have suggested that the northern Nevada rift may have been localized by a pre-Cenozoic structure (e.g., Wooden et al., 1998; Theodore et al., 1998; John et al., 2000). If this is the case, then it is plausible that the orientation of the rift may simply reflect the orientation of this structure or structures, rather than the regional extension direction. There is a growing body of data documenting middle Miocene extension (contemporaneous with the northern Nevada rift) across a wide area of the northern Basin and Range (e.g., McQuarrie and Wernicke, 2005, and references therein). Significantly, the kinematic data compiled by McQuarrie and Wernicke (2005) demonstrate that extension across the northern and central Basin and Range was oriented approximately N78°W, much closer to the N80°W documented by this study than to the N70°E direction indicated by the northern Nevada Rift.

APPENDIX A. $^{40}Ar/^{39}Ar$ ANALYTICAL METHODS

Samples for $^{40}Ar/^{39}Ar$ dating were irradiated for 16 hours in the U.S. Geological Survey TRIGA Reactor Facility in Denver, Colorado. An intralaboratory standard sanidine, TCR-2 (Taylor Creek Rhyolite), was used for calculation of the neutron flux in all irradiations. Decay and abundance constants for all ages reported are those recommended by Steiger and Jäger (1977). Ages in Table 3 and Table A1 were recalculated to an age of 28.02 Ma for Fish Canyon Tuff sanidine standard (Renne et al., 1998).

$^{40}Ar/^{39}Ar$ ages reported in Table 3 were obtained by laser-fusion analyses on 4 to 8 crystals of sanidine separated from each sample by standard separation techniques. Laser-fusion $^{40}Ar/^{39}Ar$ dating is especially useful to detect and overcome the effects of xenocrystic contamination (LoBello et al., 1987; Fleck and Carr, 1990) and incomplete extraction of radiogenic Ar from alkali feldspar (McDowell, 1983). Multiple splits of each sample were analyzed and ages and uncertainties reported are the weighted mean and standard error of these analyses. Outliers related to contamination are identifiable from the bulk of the analyses and are omitted. Ages reported for each sample are represented by the weighted means of replicate laser-fusion analyses, with the inverse variance of propagated, within-run (i.e., "internal") errors used as the weighting factors (Taylor, 1982). The goodness of fit parameter, mean square of weighted deviates (MSWD; McIntyre et al., 1966), is calculated for these means and is used to determine the presence of any error component in excess of estimated analytical error (an "external" error). Where the MSWD of a mean is greater than 1.0, analytical errors are multiplied by the square root of MSWD, as discussed by Ludwig (2003) and Fleck et al. (1996), to incorporate this error.

$^{40}Ar/^{39}Ar$ ages reported for whole-rock basalts in Table A1 were obtained by incremental-heating analysis, i.e., sequential extraction of the argon from the sample at progressively higher temperatures until the sample is fused. Samples were crushed and sized to between 250 and 180 micrometers and wrapped in Cu packets for irradiation. Incremental-heating analyses utilized a low-blank, tantalum and molybdenum, resistance-heated furnace, commonly releasing all of the Ar in 8 to 15 temperature-controlled heating increments. Reported ages are $^{40}Ar/^{39}Ar$ plateau ages, defined as the weighted mean ages of contiguous gas fractions representing more than 50% of the ^{39}Ar released for which no difference can be detected between the ages of any two fractions at the 95% level of confidence (Fleck et al., 1977).

ACKNOWLEDGMENTS

This research was supported by a U.S. Geological Survey Mendenhall Postdoctoral Research Fellowship to Colgan. We thank Barrick Gold Corporation for access to the Pipeline, Toiyabe, and Cortez Mine sites, and for sharing subsurface data and samples. Mike Perkins provided tephra correlations from his extensive database. Conversations and field work with Alan Wallace, Tom Moore, and Keith Howard helped to clarify the ideas presented here. We thank Keith Howard, Tom Chapin, and Sherman Gromme for comments on an earlier version of the manuscript, and Alan Wallace and David Rodgers for thorough journal reviews.

REFERENCES CITED

Armstrong, R.L., 1970, Geochronology of Tertiary igneous rocks, eastern Basin and Range Province, western Utah, eastern Nevada, and vicinity, U.S.A: Geochimica et Cosmochimica Acta, v. 34, p. 203–232, doi: 10.1016/0016-7037(70)90007-4.

Bennett, R.A., Wernicke, B.P., Niemi, N.A., Friedrich, A.M., and Davis, J.L., 2003, Contemporary strain rates in the northern Basin and Range province from GPS data: Tectonics, v. 22, 1008, p. 1–29, doi: 10.1029/2001TC001355.

Bingler, E.C., 1978, Abandonment of the name Hartford Hill Rhyolite Tuff and adoption of new formation names for middle Tertiary ash-flow tuffs in the Carson City-Silver City area, Nevada: U.S. Geological Survey Bulletin 1457-D, 19 p.

Blair, T.C., and McPherson, J.G., 1994, Alluvial fans and their natural distinction from rivers based on morphology, hydraulic processes, sedimentary processes, and facies assemblages: Journal of Sedimentary Research, v. A64, p. 450–489.

Burke, D.B., and McKee, E.H., 1979, Mid-Cenozoic volcano-tectonic troughs in central Nevada: Geological Society of America Bulletin, v. 90, part 1, p. 181–184, doi: 10.1130/0016-7606(1979)90<181:MVTICN>2.0.CO;2.

Colgan, J.P., and Metcalf, J.R., 2006, Apatite fission-track

TABLE A1: $^{40}Ar/^{39}Ar$ INCREMENTAL HEATING DATA

Sample: 00DJ-1, Whole Rock Basalt	Lat: 40°10′56?N	Long: 116°30′12?W	Irradiation: IRR166-4	J = 0.00428805			
Step (°C)	% ^{39}ArK Rel	% ^{40}Ar*	$^{40}Ar/^{39}Ar$	$^{37}Ar/^{39}Ar$	$^{36}Ar/^{39}Ar$	K/Ca	Cl/K	Age (Ma, ±1?)
550	0.63	29.47	8.63907	3.56665	2.1538E-02	0.137		*19.637 ± 0.985*
625	4.90	62.92	3.97329	1.79484	5.4339E-03	0.273		*19.258 ± 0.181*
700	8.49	73.83	3.14107	1.97962	3.2784E-03	0.247		*17.875 ± 0.135*
775	10.48	70.23	3.10471	1.93648	3.6127E-03	0.253		*16.811 ± 0.124*
850	14.15	84.18	2.52867	1.50837	1.7249E-03	0.325		16.409 ± 0.109
900	12.26	88.62	2.38171	1.31476	1.2371E-03	0.372		16.268 ± 0.109
950	10.62	86.50	2.46387	1.22982	1.4227E-03	0.398		16.425 ± 0.114
1000	10.93	80.75	2.63492	0.93298	1.9351E-03	0.525		16.394 ± 0.115
1075	12.33	75.29	2.81209	1.20843	2.6430E-03	0.405		16.317 ± 0.131
1150	5.34	60.44	3.49324	7.09681	6.5348E-03	0.069		16.336 ± 0.226
1225	5.67	56.99	3.69852	7.40628	7.3240E-03	0.066		16.312 ± 0.220
1350	4.20	59.04	3.62111	5.81123	6.5355E-03	0.084		16.527 ± 0.269
					Plateau age (Ma, ±2?)	MSWD = 0.27		16.36 ± 0.05
					Isochron age (Ma, ±2?)	MSWD = 7.1		16.35 ± 0.09

Sample: 00DJ-2, Whole-Rock Basalt	Lat: 40°07′08?N	Long: 116°30′26?W	Irradiation: IRR166-5	J = 0.00421173			
Step (°C)	% ^{39}ArK Rel	% ^{40}Ar*	$^{40}Ar/^{39}Ar$	$^{37}Ar/^{39}Ar$	$^{36}Ar/^{39}Ar$	K/Ca	Cl/K	Age (Ma, ±1?)
550	2.07	55.80	3.57266	1.03657	5.5895E-03	0.472		*15.275 ± 0.537*
625	13.58	73.63	2.88598	1.42050	2.9233E-03	0.345		*16.281 ± 0.131*
700	25.12	80.02	2.71629	1.59179	2.2302E-03	0.307		16.654 ± 0.112
750	20.25	83.59	2.60751	1.89801	1.9226E-03	0.258		16.705 ± 0.116
800	15.16	86.22	2.51372	2.46546	1.7982E-03	0.198		16.616 ± 0.156
850	10.59	83.77	2.50323	3.21770	2.2008E-03	0.152		*16.088 ± 0.197*
900	5.89	76.72	2.66284	4.16674	3.1762E-03	0.117		*15.685 ± 0.322*
975	3.26	66.48	2.83744	5.01555	4.5225E-03	0.097		*14.497 ± 0.562*
976	0.87	67.31	2.66066	5.02382	4.2499E-03	0.097		*13.765 ± 0.47*
1075	2.34	52.11	2.37053	7.37284	5.7730E-03	0.066		*9.521 ± 0.195*
1200	0.88	31.66	4.18851	99.28629	3.6068E-02	0.005		*10.903 ± 0.919*
					Plateau age (Ma, ±2?)	MSWD = 0.27		16.67 ± 0.14
					Isochron age (Ma, ±2?)	MSWD = 4.7		16.70 ± 0.32

Note: Ages in italics excluded from plateau age.

and (U-Th)/He dating of slip on the Crescent Fault, Nevada: American Geophysical Union, Fall meeting, abs. T11D-0466.

Deino, A.L., 1989, Single crystal $^{40}Ar/^{39}Ar$ dating as an aid in correlation of ash flows: Examples from the Chimney Springs/New Pass Tuffs and the Nine Hill/Bates Mountain Tuffs of California and Nevada: New Mexico Bureau of Mines and Mineral Resources: Continental Magmatism Abstracts Bulletin, v. 131, p. 70.

Dickinson, W.R., 1991, Tectonic setting of faulted Tertiary strata associated with the Catalina core complex in southern Arizona: Geological Society of America Special Paper 264, 106 p.

Dickinson, W.R., 2006, Geotectonic evolution of the Great Basin: Geosphere, v. 2, p. 353–368, doi: 10.1130/GES00054.1.

Doebrich, J.L., 1995, Geology and mineral deposits of the Antler Peak 7.5 minute quadrangle, Lander County, Nevada: Nevada Bureau of Mines and Geology Bulletin 109, scale 1:24,000, 44 p.

Faulds, J.E., and Varga, R., 1998, The role of accommodation zones and transfer zones in the regional segmentation of extended terranes, *in* Faulds, J.E., and Stewart, J.H., eds., Accommodation zones and transfer zones: The regional segmentation of the Basin and Range Province: Geological Society of America Special Paper 323, p. 1–46.

Faulds, J.E., Henry, C.D., and dePolo, C.M., 2003, Preliminary geologic map of the Tule Peak Quadrangle, Washoe County, Nevada: Nevada Bureau of Mines and Geology Open-File Report 03-10, scale 1:24,000.

Fleck, R.J., and Carr, M.D., 1990, The age of the Keystone thrust: Laser-fusion $^{40}Ar/^{39}Ar$ dating of foreland basin deposits, southern Spring Mountains, Nevada: Tectonics, v. 9, p. 467–476.

Fleck, R.J., Sutter, J.F., and Elliot, D.H., 1977, Interpretation of discordant $^{40}Ar/^{39}Ar$ age-spectra from Antarctica: Geochimica et Cosmochimica Acta, v. 41, p. 15–32.

Fleck, R.J., Turrin, B.D., Sawyer, D.A., Warren, R.G., Champion, D.E., Hudson, M.R., and Minor, S.A., 1996, Age and character of basaltic rocks of the Yucca Mountain region, southern Nevada: Journal of Geophysical Research, v. 101, no. B4, p. 8205–8227, doi: 10.1029/95JB03123.

Fosdick, J.C., and Colgan, J.P., 2008, Miocene extension in the East Range, Nevada: A two-stage history of faulting in the northern Basin and Range: Geological Society of America Bulletin, v. 120, doi: 10.1130/B26201.1 (in press).

Friedrich, A.M., Lee, J., Wernicke, B.P., and Sieh, K., 2004, Geologic context of geodetic data across a Basin and Range normal fault, Crescent Valley, Nevada: Tectonics, v. 23, TC2015, doi: 10.1029/2003TC001528.

Gans, P.B., 1987, An open-system, two-layer crustal stretching model for the eastern Great Basin: Tectonics, v. 6, p. 1–12.

Gilluly, J., and Gates, O., 1965, Tectonic and igneous geology of the northern Shoshone Range, Nevada, with sections on gravity in Crescent Valley by D. Plouff and economic geology by K.B. Ketner: U.S. Geological Survey Professional Paper 465, 135 p.

Gilluly, J., and Masursky, H., 1965, Geology of the Cortez Quadrangle, Nevada: U.S. Geological Survey Bulletin 1175, 117 p.

Gonsior, Z.J., and Dilles, J.H., 2008, The timing and evolution of Cenozoic extensional normal faulting and magmatism in the southern Tobin Range, Nevada: Geosphere, v. 4, doi: 10.1130/GES00137.1 (in press).

Henry, C.D., 2008, Ash-flow tuffs and paleovalleys in northeastern Nevada: Implications for Eocene paleogeography and extension in the Sevier hinterland, northern Great Basin: Geosphere, v. 4, doi: 10.1130/GES00122.1 (in press).

Henry, C.D., Faulds, J.E., dePolo, C.M., and Davis, D.A., 2004, Geology of the Dogskin Mountain Quadrangle, northern Walker Lane, Nevada: Nevada Bureau of Mines and Geology Map 148, scale 1:24,000, 13 p.

Hofstra, A.H., Snee, L.W., Rye, R.O., Folger, H.W., Phinisey, J.D., Loranger, R.J., Dahl, A.R., Naeser, C.W., Stein, H.J., and Lewchuk, M., 1999, Age constraints on Jerritt Canyon and other Carlin-type gold deposits in the western United States—Relationship to mid-Tertiary extension and magmatism: Economic Geology and the Bulletin of the Society of Economic Geologists, v. 94, p. 769–802.

John, D.A., Wallace, A.R., Ponce, D.A., Fleck, R.B., and Conrad, J.E., 2000, New perspectives on the geology and origin of the Northern Nevada rift, *in* Cluer, J.K., et al., eds., Geology and ore deposits 2000: The Great Basin and beyond: Geological Society of Nevada Symposium Proceedings, May 15–18, 2000, p. 127–154.

John, D.A., Henry, C.D., and Colgan, J.P., 2008, Magmatic and tectonic evolution of the Caetano caldera, north-central Nevada: A tilted mid-Tertiary eruptive center and source of the Caetano Tuff: Geosphere, v. 4, p.75–106, doi: 10.1130/GES00116.1.

Leeder, M.R., and Gawthorpe, R.L., 1987, Sedimentary models for extensional tilt-block/half graben basins, *in* Coward, M.P., et al., eds., Continental extensional

tectonics: Geological Society [London] Special Publication 28, p. 139–152.
LoBello, P., Feraud, G., Hall, C.M., York, D., Lavina, P., and Bernat, M., 1987, $^{40}Ar/^{39}Ar$ step-heating and laser fusion dating of a Quaternary pumice from Neschers, Massif Central, France: The defeat of xenocrystic contamination: Chemical Geology, v. 66, p. 61–71.
Ludwig, K.R., 2003, User's Manual for ISOPLOT 3.0, a geochronological tool kit for Microsoft Excel: Berkeley Geochronology Center Special Publication No. 4, 70 p.
Masursky, H., 1960, Welded tuffs in the northern Toiyabe Range, Nevada, *in* Geological Survey research 1960: U.S. Geological Survey Professional Paper 400B, p. B281–B283.
McClaughry, J.D., and Gaylord, D.R., 2005, Middle Eocene sedimentary and volcanic infilling of an evolving supradetachment basin: White Lake Basin, south-central British Columbia: Canadian Journal of Earth Sciences, v. 42, p. 49–66, doi: 10.1139/e04-105.
McDowell, F.W., 1983, K-Ar dating—Incomplete extraction of radiogenic argon from alkali feldspar: Isotope Geoscience, v. 1, p. 119–126.
McIntyre, G.A., Brooks, C., Compston, W., and Turek, A., 1966, The statistical assessment of Rb-Sr isochrons: Journal of Geophysical Research, v. 71, p. 5459–5468.
McKee, E.H., 1970, Fish Creek Mountains Tuff and volcanic center, Lander County, Nevada: U.S. Geological Survey Professional Paper 681, 17 p.
McKee, E.H., and Conrad, J.E., 1987, Geologic map of the Desatoya Mountains Wilderness Study Area, Churchill and Lander counties, Nevada: U.S. Geological Survey Miscellaneous Field Studies Map MF-1944, scale 1:62,500.
McQuarrie, N., and Wernicke, B.P., 2005, An animated tectonic reconstruction of southwestern North America since 36 Ma: Geosphere, v. 1, p. 147–172, doi: 10.1130/GES00016.1.
Merriam, C.W., and Anderson, C.A., 1942, Reconnaissance survey of the Roberts Mountains, Nevada: Geological Society of America Bulletin, v. 65, p. 1284–1285.
Miller, E.L., Gans, P.B., and Garing, J., 1983, The Snake Range decollement: An exhumed mid-Tertiary ductile-brittle transition: Tectonics, v. 2, p. 239–263.
Miller, E.L., Miller, M.M., Stevens, C.H., Wright, J.E., and Madrid, R., 1992, Late Paleozoic paleogeographic and tectonic evolution of the Western U.S. Cordillera, *in* Burchfield, B.C., et al., eds., The Cordilleran orogen: Conterminous U.S.: Boulder, Colorado, Geological Society of America, Geology of North America, v. G-3, p. 57–106.
Miller, J.M.G., and John, B.E., 1999, Sedimentation patterns support seismogenic low-angle normal faulting, southeastern California and Arizona: Geological Society of America Bulletin, v. 111, p. 1350–1370, doi: 10.1130/0016-7606(1999)111<1350:SPSSLA>2.3.CO;2.
Moore, T.E., Murchey, B.L., and Harris, A.G., 2000, Significance of geologic and biostratigraphic relations between the overlap assemblage and Havallah sequence, southern Shoshone Range, Nevada, *in* Cluer, K.J., et al., eds., Geology and ore deposits 2000: The Great Basin and beyond: Geological Society of Nevada Symposium Proceedings, May 15–18, 2000, p. 397–418.
Moore, T.E., O'Sullivan, P.B., Murchey, B.L., Moring, B.C., Harris, A.G., Blodgett, R.B., and Fleck, R.J., 2005, Geologic map of The Cedars quadrangle, southern Shoshone Range, Nevada: Window to the world: Geological Society of Nevada Symposium Proceedings, May 14–18, Reno, Nevada, p. 67.
Muffler, L.J.P., 1964, Geology of the Frenchie Creek quadrangle, north-central Nevada: U.S. Geological Survey Bulletin 1179, scale 1:62,500, 99 p.
Muntean, J.L., 2006, Major precious-metal deposits, *in* The Nevada mineral industry—2005: Nevada Bureau of Mines and Geology Special Publication MI-2005, p. 29–51.
Muntean, J., Tarnocai, C., Coward, M., Rouby, D., and Jackson, A., 2001, Styles and restorations of Tertiary extension in north-central Nevada, *in* Shaddrick, D.R., et al., eds., Regional tectonics and structural control of ore: The major gold trends of northern Nevada: Geological Society of Nevada Special Publication 33, p. 55–69.
Niemi, N.A., Wernicke, B.P., Friedrich, A.M., Simons, M., Bennett, R.A., and Davis, J.L., 2004, BARGEN continuous GPS data across the eastern Basin and Range province, and implications for fault system dynamics: Geophysical Journal International, v. 159, p. 842–862, doi: 10.1111/j.1365-246X.2004.02454.x.
Perkins, M.E., and Nash, B.P., 2002, Explosive silicic volcanism of the Yellowstone hotspot: The ash-fall tuff record: Geological Society of America Bulletin, v. 114, p. 367–381, doi: 10.1130/0016-7606(2002)114<0367:ESVOTY>2.0.CO;2.
Perkins, M.E., Brown, F.H., Nash, W.P., McIntosh, W., and Williams, S.K., 1998, Sequence, age, and source of silicic fallout tuffs in middle to late Miocene basins of the northern Basin and Range province: Geological Society of America Bulletin, v. 110, p. 344–360, doi: 10.1130/0016-7606(1998)110<0344:SAASOS>2.3.CO;2.
Proffett, J.M., Jr., 1977, Cenozoic geology of the Yerington District, Nevada, and implications for the nature and origin of Basin and Range faulting: Geological Society of America Bulletin, v. 88, p. 247–266, doi: 10.1130/0016-7606(1977)88<247:CGOTYD>2.0.CO;2.
Racheboeuf, P.R., Moore, T.E., and Boldgett, R.B., 2004, A new species of *Dyoros* (brachiopoda, chonetoidea) from Nevada (United States) and stratigraphic implication for the Pennsylvanian and Permian Antler overlap assemblage: Geobios, v. 37, p. 382–394, doi: 10.1016/j.geobios.2003.03.011.
Regnier, J., 1960, Cenozoic geology in the vicinity of Carlin, Nevada: Geological Society of America Bulletin, v. 71, p. 1189–1210, doi: 10.1130/0016-7606(1960)71[1189:CGITVO]2.0.CO;2.
Renne, P.R., Swisher, C.C., Deino, A.L., Karner, D.B., Owens, T.L., and DePaolo, D.J., 1998, Intercalibration of standards, absolute ages and uncertainties in $^{40}Ar/^{39}Ar$ dating: Chemical Geology, v. 145, p. 117–152, doi: 10.1016/S0009-2541(97)00159-9.
Ressel, M.W., and Henry, C.D., 2006, Igneous geology of the Carlin Trend, Nevada: Development of the Eocene plutonic complex and significance for Carlin-type gold deposits: Economic Geology and the Bulletin of the Society of Economic Geologists, v. 101, p. 347–383.
Roberts, R.J., 1951, Geology of the Antler Peak quadrangle, Nevada: U.S. Geological Survey Quadrangle Map GQ-10, scale 1:25,000.
Roberts, R.J., Ferguson, H.G., Gilluly, J., and Hotz, P.E., 1958, Paleozoic rocks of north-central Nevada: American Association of Petroleum Geologists Bulletin, v. 42, p. 2813–2857.
Sharp, R.P., 1939, The Miocene Humboldt Formation in northeastern Nevada: Journal of Geology, v. 47, no. 2, p. 133–160.
Smith, F.J., and Ketner, K.B., 1976, Stratigraphy of post-Paleozoic rocks and summary of resources in the Carlin-Pinon Range area, Nevada: U.S. Geological Survey Professional Paper 867-B, 48 p.
Sohn, Y.K., Rhee, C.W., and Kim, B.C., 1999, Debris flow and hyperconcentrated flood-flow deposits in an alluvial fan, northwestern part of the Cretaceous Yongdong Basin, central Korea: Journal of Geology, v. 107, p. 111–132, doi: 10.1086/314334.
Steiger, R.H., and Jäger, E., 1977, Subcommission on geochronology: Convention on the use of decay constants in geo- and cosmochronology: Earth and Planetary Science Letters, v. 36, p. 359–362, doi: 10.1016/0012-821X(77)90060-7.
Stewart, J.H., and Carlson, J.E., compilers, 1978, Geologic map of Nevada: U.S. Geological Survey State Geologic Map, scale 1:500,000.
Stewart, J.H., and McKee, E.H., 1968, Geologic map of the Mount Callaghan Quadrangle, Lander County, Nevada: U.S. Geological Survey Quadrangle Map GQ-730, scale 1:62,500.
Stewart, J.H., and McKee, E.H., 1977, Geology and mineral deposits of Lander County, Nevada: U.S. Geological Survey Bulletin 88, scale 1:250,000, 114 p.
Taylor, J.R., 1982, An introduction to error analysis: The study of uncertainties in physical measurements: Mill Valley, California, University Science Books, 270 p.
Theodore, T.G., Armstrong, A.K., Harris, A.G., Stevens, C.H., and Tosdal, R.M., 1998, Geology of the northern terminus of the Carlin trend, Nevada—Links between crustal shortening during the late Paleozoic Humboldt orogeny and northeast-striking faults, *in* Tosdal, R.M., ed., Contributions to the gold metallogeny of northern Nevada: U.S. Geological Survey Open-File Report 98-338, p. 69–105.
Thompson, G.A., 1960, Problem of the late Cenozoic structure of the Basin Ranges: Proceedings, International Geological Congress, 21st, Copenhagen, Session 18, p. 62–68.
Wallace, A.R., Perkins, M.E., and Fleck, R.J., 2008, Late Cenozoic paleogeographic evolution of northeastern Nevada: Evidence from the sedimentary basins: Geosphere, v. 4, p. 36–74 doi: 10.1130/GES00114.1.
Wesnousky, S.G., Barron, A.D., Briggs, R.W., Caskey, J.S., Kumar, S., and Owen, L., 2005, Paleoseismic transect across the northern Great Basin: Journal of Geophysical Research, v. 110, B05408, doi: 10.1029/2004JB003283.
Whipple, K.X., and Dunne, T., 1992, The influence of debris-flow rheology on fan morphology, Owens Valley, California: Geological Society of America Bulletin, v. 104, p. 887–900, doi: 10.1130/0016-7606(1992)104<0887:TIODFR>2.3.CO;2.
Wooden, J.L., Kistler, R.W., and Tosdal, R.M., 1998, Pb isotopic mapping of crustal structure in the northern Great Basin and relationships to Au deposit trends, *in* Tosdal, R.M., ed., Contributions to the gold metallogeny of northern Nevada: U.S. Geological Survey Open-File Report 98-338, p. 20–33.
Zoback, M.L., and Thompson, G.A., 1978, Basin and Range rifting in northern Nevada: Clues from a mid-Miocene rift and its subsequent offsets: Geology, v. 6, p. 111–116, doi: 10.1130/0091-7613(1978)6<111:BARRIN>2.0.CO;2.
Zoback, M.L., McKee, E.H., Blakely, R.J., and Thompson, G.A., 1994, The northern Nevada rift: Regional tectonomagmatic relations and middle Miocene stress direction: Geological Society of America Bulletin, v. 106, p. 371–382, doi: 10.1130/0016-7606(1994)106<0371:TNNRRT>2.3.CO;2.

Manuscript Received 30 March 2007
Revised Manuscript Received 6 September 2007
Manuscript Accepted 7 September 2007